Prediction and validation of distinct temporal dynamics of transient and sustained ERK activation

（一過性及び持続性 ERK 活性化ダイナミクスの予測と実証）

Yu-ichi Ozaki

Acknowledgements

First of all, I appreciate my supervisors Assoc. Prof. Shinya Kuroda for guiding me through the interesting fields of systems biology. I am grateful for his supervision, guidance, suggestions and invaluable encouragement throughout the development of this thesis. I am gratefull to my colleague Dr. Satoru Sasagawa for his close cooperation, and especially for his massive experiments. I am grateful to my colleague Kazuhiro Fujita for helpful discussions and contributions. I thank Kozo Kaibuchi, Yukiko Gotoh, Mitsuo Kawato and Masanori Arita for critically reading the manuscript that was the basis of this thesis, and Ranko Kettunen and Risa Kunihiro for their technical assistance. I am grateful to my thesis committee members, Prof. Toshihisa Takagi, Prof. Shinichi Morishita, Prof. Takashi Ito, Assoc. Prof. Mikihiko Naito, and Assoc. Prof. Shinya Kuroda, for the time and effort they expended in reviewing my work and making suggestions for its improvement. This work was supported in part by a grant in-aid for scientific research from the Ministry of Education, Culture, Sports, Science and Technology of Japan, and by a grant in-aid from Uehara Memorial Foundation. Most of all I would like to thank to my wife, Tomoko, for her love and support.

Contents

Acknowledgements

1 Introduction **3**

2 Results **7**

3 Discussion and Conclusions **20**

Methods **28**

Reference **32**

Figures **37**

Appendix A **50**

Appendix B **53**

This thesis is the result of the joint research of Dr. Satoru Sasagawa, Kazuhiro Fujita, Dr. Shinya Kuroda and the author. The author accomplished the development and analysis of *in silico* and simple models. The author also performed *in vivo* experiments of Figure 2, and a part of preliminary experiments of Figure 1. Dr. Sasagawa accomplished most of the *in vivo* experiments, and the construction of the block diagram around TrkA. Fujita made Figure 6c and d, and performed sensitivity analysis of the *in silico* model. These works were organized under the guidance of Dr. Kuroda.

Introduction

Signal transduction networks, including ERK (extracellular signal-regulated kinase) networks, are known to regulate multiple cellular functions. In general, such multiplicity of signal transduction networks is achieved by cooperativity of several signalling molecules and networks. Such multiplicity can be produced by distinct temporal pattern coding mechanisms of the same signalling networks. This feature is an important characteristic of signal transduction systems. The same ERK signalling network can elicit distinct functions via distinct temporal activation patterns. For example, in PC12 cells, transient and sustained activation of ERK have been shown to lead to proliferation and differentiation, respectively (Vaudry et al., 2002). However, how the signalling network converts extracellular information into distinct temporal activation patterns of a certain molecule remains unknown. Therefore, the purpose of this thesis is to explore the encoding systems of distinct extracellular information into transient and sustained ERK activation.

In PC12 cells, extracellular stimuli such as epidermal growth factor (EGF) and nerve growth factor (NGF) regulate cell-fate decisions by transient, and transient and sustained ERK activation, respectively (Gotoh et al., 1990; Qiu and Green, 1992; Traverse et al., 1992; Vaudry et al., 2002). EGF-dependent ERK activation involves tyrosine phosphorylation of the EGF receptor (EGFR) accompanied by association with Grb2-SOS (Egan et al., 1993; Gale et al., 1993; Li et al., 1993; Rozakis-Adcock et al., 1993), SOS-dependent Ras activation (Egan et al., 1993; Gale et al., 1993; Li et al., 1993; Rozakis-Adcock et al., 1993) followed by activation of Raf and mitogen-activated protein- or ERK-kinase (MEK), leading to ERK activation (Davis, 1993). In turn, ERK activation is terminated by EGFR internalisation followed by degradation (Di Fiore and Gill, 1999; Waterman and Yarden, 2001), recruitment of Ras GTPase-activating protein

(GAP) to the tyrosine phosphorylated receptors (Jones and Dumont, 1999; Soler et al., 1993), and ERK-dependent feedback inhibition of SOS (Dong et al., 1996; Waters et al., 1995), resulting in transient ERK activation. NGF-dependent ERK activation consists of transient and sustained ERK activation. NGF transmits the signals downstream via tyrosine phosphorylation of TrkA, a subunit of NGFR (Vaudry et al., 2002). Transient ERK activation by NGF depends on Ras, similar to EGF-dependent ERK activation (Marshall, 1998). Sustained ERK activation involves slow and sustained activation of Rap1 (Kao et al., 2001; Marshall, 1998; Wu et al., 2001; York et al., 1998) mediated by sustained TrkA activation (Chang et al., 2003). Activated Rap1 activates B-Raf followed by activation of MEK and ERK (Ohtsuka et al., 1996; Vossler et al., 1997). The sustained TrkA and Rap1 activation results in the sustained ERK activation (Marshall, 1998; York et al., 1998). Recent studies have provided practical molecular frameworks of EGF- and NGF-dependent ERK signalling networks (Kao et al., 2001; Vaudry et al., 2002; Wu et al., 2001).

EGF- and NGF-dependent cell proliferation and differentiation via the same ERK signalling networks requires the specific encoding mechanisms of distinct physical information of EGF and NGF into transient, and transient and sustained ERK activation, respectively. However, it is difficult to understand the mechanism of such encoding systems based on the accumulation of individual knowledge without quantitative models (Bhalla and Iyengar, 1999). To address this issue, we took advantage of kinetic computer simulation models. Theoretical analysis of *in silico* models enables us to extract essential and simple frameworks of the characteristics of the complex ERK signalling networks (Heinrich et al., 2002). Several computational models of ERK signalling networks have been proposed for EGF dependent transient ERK activation

(Bhalla and Iyengar, 1999; Bhalla et al., 2002; Brightman and Fell, 2000; Hatakeyama et al., 2003; Schoeberl et al., 2002; Shvartsman et al., 2002; Yamada et al., 2004), however, these models cannot account for the distinct encoding systems of EGF and NGF into transient, and transient and sustained ERK activation, respectively. Moreover, recent identification of additional signalling networks and detailed observation have made it clear that the existing models cannot consistently explain even some aspect of transient ERK activation. To understand the encoding systems of the distinct physical information of EGF and NGF into transient, and transient and sustained ERK activation, respectively, we made an integrated approach between *in silico* kinetic simulation and *in vivo* dynamics measurement in PC12 cells. Because the *in vivo* dynamics of signalling networks differ between cell lines due to differences in critical parameters such as the expression level of molecules, the *in silico* dynamics should be constrained by the *in vivo* dynamics in a single cell line. Furthermore, the ERK signalling networks have several cross-talk points (molecules) that are cooperatively regulated by upstream or downstream networks. It is important to measure the activities of these points in dose- and temporal-dependent manners in growth factors because the dynamics of the cross-talk points of ERK signalling networks critically determine the dynamics of the whole network (Bruggeman et al., 2002).

Therefore, we developed a kinetic simulation model of EGF- and NGF-dependent ERK signalling networks by constraining the *in silico* dynamics of the cross-talk points of the ERK signalling networks based on the *in vivo* dynamics measurement in a single cell line, PC12 cells, in dose- and temporal-dependent manners in growth factors. Measured *in vivo* dynamics can be consistently reproduced in dose- and temporal-dependent manners in growth factors *in silico*. Using this *in vivo* validated model, we

predicted *in silico* and validated *in vivo* that the Ras and Rap1 systems specifically capture the temporal rate and concentration of growth factors, and encode these distinct physical properties of growth factors into transient and sustained ERK activation, respectively.

1. Results

In silico model of ERK signalling networks based on *in vivo* dynamics measurements

Based on the literature, we first developed a block diagram of ERK signalling networks (Fig. 1a, see Appendix B, Fig. S1). The block diagram consists of EGF- and NGF-dependent receptor complex formation with adaptor proteins, the internalisation of the receptors and ubiquitination of EGF receptor (EGFR), Ras and Rap1 activation, and MEK and ERK phosphorylation (Fig. S1). We determined kinetic parameters based on earlier experimental observations and some assumptions, then further constrained parameters on the basis of *in vivo* dynamics in a single cell line, PC12 cells (see Appendix B, Table S1).

We first measured *in vivo* dynamics of the cross-talk points of the ERK signalling networks in dose- and temporal-dependent manners in EGF and NGF. We measured the *in vivo* tyrosine phosphorylation of EGFR and TrkA in response to EGF and NGF, respectively, because constant stimulation of growth factors is first transformed into different temporal patterns at the receptor level (Fig. 1a, boxes). The *in vivo* tyrosine phosphorylation of EGFR and TrkA was increased in a dose-dependent manner in EGF and NGF in PC12 cells, while the tyrosine phosphorylation of EGFR and TrkA were transient and sustained, respectively (Fig. 1b, c, upper panels, see Appendix B, Fig. S2) (Kao et al., 2001; Kholodenko et al., 1999; Wu et al., 2001). On the basis of *in vivo* dynamics, we constrained the *in silico* tyrosine phosphorylation of both receptors (Fig. 1b, c, lower panels). Upon the EGF and NGF stimulation, SOS is recruited to the plasma membrane where SOS activates Ras (Downward, 1994), and it is subsequently

inhibited by ERK-dependent phosphorylation (Holt et al., 1996; Langlois et al., 1995). The phosphorylation of SOS by ERK leads to the dissociation of SOS from the complex with Grb2, resulting in decline of Ras activation (Holt et al., 1996; Langlois et al., 1995). Thus, SOS is a cross-talk point of ERK-dependent negative feedback inhibition (Holt et al., 1996; Langlois et al., 1995) (see below). Mobility shifts in SOS reflect its phosphorylation state, which can be regarded as an inactive state of SOS (Holt et al., 1996; Langlois et al., 1995). The *in vivo* mobility shift of SOS in response to EGF was transient (Fig. 1d, upper panel), whereas that in response to NGF was sustained (Fig. 1e, upper panel) (Kao et al., 2001). These SOS mobility shifts were correlated with ERK activation (Holt et al., 1996; Langlois et al., 1995) (Fig. 1h, i). On the basis of the *in vivo* dynamics, we constrained *in silico* phosphorylation of SOS (Fig. 1d, e, lower panels). Signals downstream of the receptors diverge into Ras and Rap1 activities, then merge again into ERK activation (Marshall, 1998; York et al., 1998) via successive Raf and MEK activation (Davis, 1993; Nishida and Gotoh, 1993). These small GTPases are activated by the conversion of GDP-bound forms to GTP-bound forms (Bourne et al., 1991). The *in vivo* activation of Ras was transient in response to both stimuli (Fig. 1f, upper panel, Fig. S2) (Kao et al., 2001; Wu et al., 2001). The EGF stimulus did not induce sufficient activation of Rap1, whereas the NGF stimulus induced sustained activation of Rap1 (Fig. 1g, upper panel, Fig. S2) (Kao et al., 2001; Wu et al., 2001). This distinct activation of Ras versus Rap1 is responsible for transient and sustained activation of ERK, respectively (Marshall, 1998; York et al., 1998). We constrained the *in silico* dynamics of Ras and Rap1 (Fig. 1f, g, lower panels), which are dependent on the distinct mechanisms of their activation and inhibition processes (see below). The *in vivo* basal level of Rap1 activity was higher than that *in silico*. This may be due to the

higher basal C3G activity or the lower basal Rap1GAP activity *in vivo* compared to that *in silico*, or to the basal non-specific binding of Rap1 to the beads. Signals from EGF and NGF via Ras- and Rap1-mediated networks are transformed into transient, and transient and sustained ERK activation through Raf and MEK, respectively. The activation of ERK depends on phosphorylation by MEK (Davis, 1993; Nishida and Gotoh, 1993). The EGF stimulus induced transient ERK phosphorylation *in vivo* (Fig. 1h, upper panel, Fig. S2), whereas the NGF stimulus induced transient and sustained ERK phosphorylation *in vivo* (Fig. 1i, upper panel, Fig. S2) (Kao et al., 2001; Wu et al., 2001). We constrained the *in silico* dynamics of transient and sustained ERK phosphorylation (Fig. 1h, i, lower panels). In this model, the EGF- and NGF-dependent transient ERK activation disappeared when Ras activation was blocked, whereas the NGF-dependent sustained ERK activation disappeared when Rap1 activation was blocked (see Appendix B, Fig. S3) (York et al., 1998). Thus, *in silico*, the EGF-dependent transient ERK phosphorylation mainly depended on Ras activation, whereas the NGF-dependent transient and sustained ERK phosphorylation depended on Ras and Rap1 activation, respectively (York et al., 1998).

The *in vivo* EC_{50} value of EGF, which represents 50% of the EGF-dependent maximal transient ERK phosphorylation at 2 min after stimulation, was 1.26 ng/ml, and the EC_{50} values of NGF for transient and sustained ERK phosphorylation at 5 and 30 min after stimulation were 1.13 and 2.31 ng/ml, respectively. The *in silico* EC_{50} value of EGF for the transient ERK phosphorylation was 1.39 ng/ml, and the EC_{50} values of NGF for the transient and sustained ERK phosphorylation were 1.36 and 3.06 ng/ml, respectively. The similarity between the *in vivo* and *in silico* EC_{50} values of growth factors for the transient and sustained ERK phosphorylation supports the high fidelity of

the *in silico* dynamics of the ERK signalling network from growth factors to ERK. In addition, this *in silico* model successfully reproduced the following *in vivo* experimental observations. The transient ERK activation did not always correlate with tyrosine phosphorylation of EGFR, especially at low doses of EGF (Fig. 1b, h). The sustained ERK activation was nearly proportional to the tyrosine phosphorylation of TrkA (Fig. 1c, i, see below). Inactivation of Ras was much faster than that of the SOS phosphorylation (Fig. 1d-f).

We used the above *in vivo* dynamics to fix the parameters in the *in silico* model (Table S1) and further examined the temporal dynamics of the ERK signalling networks without changing parameters.

In silico prediction and *in vivo* validation of the distinct temporal dynamics of transient and sustained ERK activation

Constant stimulation of growth factors is generally used for measurement of *in vivo* dynamics (Fig. 2a, b, upper panels, solid lines). However, under physiological conditions, concentrations of growth factors are likely to gradually increase in a spatiotemporal-dependent manner. Therefore, by taking advantage of our *in silico* experiment, we predicted ERK activation in response to various increasing rates of EGF and NGF (Fig. 2a, b, upper panels). Although constant EGF stimulus induced the transient ERK activation, the transient ERK activation gradually decreased as the temporal rates of EGF decreased *in silico* (Fig. 2a, middle panel). Importantly, the slow stimulus did not induce sufficient transient ERK activation (Fig. 2a, middle panel, green dashed line). In contrast, a similar sustained ERK activation was induced by both increasing and constant NGF stimuli *in silico* (Fig. 2b, middle panel). However, the

transient ERK activation gradually decreased as the temporal rates of NGF decreased. Thus, the transient ERK activation depends on the temporal rates of EGF and NGF, whereas the sustained ERK activation can respond to both increasing and constant NGF stimuli and depends on the final concentrations. This difference is due to the distinct activation mechanisms of Ras and Rap1 which are responsible for transient and sustained ERK activation, respectively (see below).

We next attempted to validate this *in silico* prediction by measuring *in vivo* dynamics. As we had predicted, the transient ERK activation decreased as the temporal rate of EGF decreased *in vivo* (Fig. 2a, lower panel, Fig. S2). The slow stimulus did not induce the sufficient transient ERK activation (Fig. 2a, lower panel, green dashed line). As the temporal rate of EGF decreased, the peak concentration of the transient ERK phosphorylation decreased *in silico* (Fig. 2c). These results indicate that the transient ERK activation depends on the temporal rate of the growth factor increase rather than the final concentration. In contrast, a similar sustained ERK activation was induced by both increasing and constant NGF stimuli *in vivo* (Fig. 2b, lower panel, Fig. S2). However, the transient ERK activation gradually decreased as the temporal rates of NGF decreased, which was also consistent with the *in silico* prediction. The sustained ERK activation depends on the final concentrations of NGF irrespective of constant or increasing stimulation *in silico* (Fig. 2d). These results indicate that sustained ERK activation depends on the final concentrations of NGF rather than on its temporal rate. However, *in silico* ERK activation decreased in the transitional state (around 30 min after NGF stimulation), whereas *in vivo* ERK activation did not decreased and reached similar levels in response to both constant and increasing NGF stimuli in the transitional state (Fig. 2b). This difference is due to the faster decay of the transient ERK activation

in silico in response to the increasing NGF stimulus as compared to that *in vivo*. Similarly, the increasing EGF stimulus also led to the faster decay of the transient ERK activation *in silico* as compared to that *in vivo* (Fig. 2a). The reason of the different decay of the ERK activation between *in silico* and *in vivo* remains unknown, but it is possible that additional unknown mechanism(s) underlie the decay of the transient ERK activation *in vivo*.

To further confirm the distinct temporal dynamics of the transient and sustained ERK activation, we performed stepwise increase and decrease of stimuli to predict *in silico* and validate *in vivo* the dynamics of the ERK activation (Fig. 3). The stepwise increase of EGF successively triggered the transient ERK activation *in silico* and *in vivo* (Fig. 3a, Fig. S2). The initial constant EGF stimulus (0.5 ng/ml) triggered the efficient transient ERK activation, and the additional constant EGF stimulus (10 ng/ml) again triggered the transient ERK activation, indicating that the rapid increase of EGF, rather than a threshold or absolute concentration, induces the transient ERK activation. A stepwise decrease of NGF, however, induced the sustained ERK activation that was similar to that seen in response to the final concentration, rather than the initial concentration, of NGF *in silico* and *in vivo* (Fig. 3b, Fig. S2) (Choi et al., 2001). These results clearly indicate that the transient ERK activation depends on the rapid temporal rates of growth factors but not on their final concentrations, whereas the sustained ERK activation depends on the final concentration of NGF but not on its temporal rate of increase. However, in response to the stepwise decrease of NGF (5 to 0 ng/ml), *in silico* ERK activation reached the basal level at 60 min, whereas *in vivo* ERK activation remained at 10%. The reason for the different decay rates of the sustained ERK activation between *in silico* and *in vivo* remains unclear, although it is possible that additional unknown

mechanism(s) underlie the decay of the sustained ERK activation *in vivo*.

Distinct temporal dynamics of Ras and Rap1 activation

We explored the mechanisms underlying the distinct dynamics of the transient and sustained ERK activation *in silico* (Fig. 4). The transient ERK activation, which requires a rapid increase of stimuli, is due to the mechanism of Ras activation. Transient Ras activation decreased as the temporal rate of growth factors decreased (Fig. 4a, lower panel). The slow EGF stimulus did not induce the sufficient transient Ras activation (Fig. 4a, green dashed line in lower panel). The transient Ras activation is determined by the balance between activation and inactivation processes. Deletion of RasGAP activity resulted in the sustained Ras activation (Fig. 5b), indicating the critical role of RasGAP in rapid termination of the transient Ras activation. Inhibition of EGFR internalisation did not affect the transient Ras activation, but led to a slight increase in the sustained Ras activation (Fig. 5c). Inhibition of ERK-dependent feedback inhibition of SOS did not affect the transient Ras activation, but led to the slight increase in the transitional Ras activation (Fig. 5d). Thus, the transient Ras activation is substantially regulated by the activity balance between SOS (Downward, 1994) (Fig. 4a, upper panel) and RasGAP (Jones and Dumont, 1999; Soler et al., 1993) (Fig. 4a, middle panel) in the *in silico* model. The rapid stimuli, as the constant stimuli, initially led to fast SOS recruitment (Fig. 4a, upper panel) and then to slow RasGAP recruitment *in silico* (Fig. 4a, middle panel), resulting in sufficient transient Ras activation *in silico* (Fig. 4a, lower panel). Although the slow stimuli led to the same processes, difference in activity between SOS and RasGAP was extended and decreased *in silico* (Fig. 4a), resulting in the disappearance of the transient Ras activation. The apparent time constants of the

SOS and RasGAP recruitment mainly depended on the time constants of binding of Shc to phosphorylated EGFR and of phosphorylation/dephosphorylation of Dok, respectively *in silico* (data not shown). The amplitudes of SOS and RasGAP recruitments mainly depended on affinities of Shc to SOS·Grb2, and of phosphorylated Dok to RasGAP, respectively, and on initial concentrations of Shc and RasGAP, respectively, *in silico* (data not shown). Because the initial rate is given by the amplitude divided by the time constant (see Appendix B, Fig. S5), the distinct rates of the SOS and RasGAP recruitments depended on these time constants, affinities and initial concentrations. Consistent with this *in silico* prediction, the *in vivo* recruitment of SOS to the membrane fraction preceded that of RasGAP in response to the constant EGF stimulus (Fig. 4c, Fig. S2). Thus, transient Ras activation depends on a temporal rate of growth factors.

In contrast to RasGAP, Rap1GAP was constant regardless of the stimuli *in silico*. An apparent negative feedback inhibition and stimuli-dependent inactivation process has not been found in the Rap1 activation process, and therefore the Rap1 activation simply responded to the C3G activity which depended on sustained TrkA phosphorylation (Fig. 4b). The inhibition of Rap1 by Rap1GAP was necessary for the NGF dose-dependent sustained ERK activation because the deletion of Rap1GAP led to the similar sustained Rap1 activation regardless of the NGF concentrations (Fig. 5e). Therefore, Rap1 can respond to both an increase and a decrease of NGF stimulus and the activation of Rap1 depends on the final concentration of NGF (Fig. 1i, Fig. 4b).

We examined the *in silico* prediction *in vivo*, and found that the sustained Rap1 activation was observed in response to both constant and increasing NGF stimuli *in vivo* (Fig. 4b, lower panel). Similar to the Ras activation, inhibition of EGFR internalisation

led to the sustained Rap1 and ERK activation *in silico* (Fig. 5f, g). The sustained Ras or Rap1 activation can lead to the sustained ERK activation (Fig. 5g). Consistent with the *in silico* prediction, we found that the sustained EGFR phosphorylation induced by EGF (10 ng/ml) in the presence of MG-132 (Longva et al., 2002), a proteasome inhibitor, increased the sustained Ras, Rap1 and ERK activation *in vivo* (see Appendix B, Fig. S4).

These results indicate that the growth factor-dependent fast SOS and slow RasGAP activation regulates the transient Ras activation, and that the constant Rap1GAP activity with the growth factor-dependent C3G activation regulates the sustained Rap1 activation.

Mechanisms of how the Ras and Rap1 systems capture the temporal rate and concentration of stimulation

To facilitate understanding how the Ras and Rap1 systems specifically capture the temporal rate and concentration of stimulation, we developed simple Ras and Rap1 models downstream of phosphorylated receptors on the basis of the above findings (Fig. 6, Appendix A). The mechanism of transient Ras activation can be simplified as follows; (i) the phosphorylated receptor (denotes by pR) activates SOS (denoted by GEF); (ii) pR activates RasGAP (denoted by GAP); (iii) these GEF and GAP activates and inactivates Ras, respectively. Furthermore, dose-responses of these regulators against pR follow first order reaction kinetics (Fig. S6). Here we assume that the series of activation processes of GEF and GAP by pR can be approximated by a single first order reaction with respect to pR. In the simple Ras model, the Ras activation and inactivation were approximated by reactions with pR·GEF and pR·GAP, respectively (Fig. 6a, eq. (5) in Appendix A). The GEF and GAP activation were approximated by

reactions with pR (Fig. 6a, eq. (3), (4) in Appendix A). We simplified the equations further by substituting variables with dimensionless variables, yielding equations (3'), (4') and (5') in the Appendix A where *GEF*, *GAP*, *Ras* and *Rap1* are dimensionless representation of pR·GEF, pR·GAP, GTP·Ras and GTP·Rap1, respectively (Appendix A). We found that the simple Ras model approximated well the *in silico* dynamics of the Ras activation (Fig. 6b red line, see also Fig. 7a) when we set p=3.5, q=0.027, Ke=3.2 and s=2, which are equivalent values in the *in silico* model (Appendix A). Here, the inverse number of q is the relative time constant of *GAP* activation compared to the *GEF* activation (Appendix A), and thereby $q < 1$ and $q > 1$ indicate the conditions where the *GEF* activation is faster and slower than the *GAP* activation, respectively. For example, the small q value (q=0.027) indicates that the SOS activation is much faster than the RasGAP activation *in silico*. The apparent transient peak of *Ras* was observed with $q < 1$, but not with $q > 1$, in response to constant *pR* stimulation (Fig. 6b). Furthermore, transient *Ras* activation, defined by $Ras_{transient}$ (Appendix B, Fig. S5), was induced in a temporal rate (r)-dependent manner in *pR* increase (Fig. 6c, Appendix A). In contrast, in the simple Rap1 model (see below), the transient *Rap1* activation was not observed under any condition (data not shown). This result supports the idea that the fast SOS and subsequent slow RasGAP activation enables the Ras system to capture the temporal rate of stimulation.

We also developed a simple Rap1 model, in which the *Rap1* activation and inactivation were approximated by reaction with pR·GEF and by reaction with the constant GAP, respectively (Fig. 6d). We derived equation (1) for the *Rap1* activation at steady state from the equations (3') and (4') (Fig. 6e, Appendix A):

$$Rap1 = \frac{pR}{(1 + K\mathrm{e})\,pR + K\mathrm{e}}, \qquad (1)$$

where *pR* is given by a constant, α (Appendix A). Under the conditions such as α << 1 where the *GEF* activation was not saturated (Appendix A, Fig. 4b, see Appendix B, Fig. S5), equation (1) can be approximated by

$$Rap1 = \frac{pR}{Ke}. \qquad (1')$$

This approximation clearly highlights the characteristics of the *Rap1* activation at steady state which is proportional to *pR*. This result supports the idea that constant Rap1GAP activity with stimulation-dependent C3G activation enables the Rap1 system to capture the final concentration of stimulation.

To compare the *Rap1* activation at steady state with that of the *Ras* activation, we derived equation (2) for the *Ras* activation at steady state (Appendix A):

$$Ras = \frac{1}{1 + pKe\dfrac{1 + pR}{1 + p \cdot pR}}, \qquad (2)$$

where *pR* is given by a constant, α, and *p* is the constant, which is the ratio of the dissociation constants between pR for GEF, and pR for GAP (Fig. 6f, Appendix A). Under the conditions of α << 1 and *p*α << 1, where the *GEF* and *GAP* activation was not saturated (Appendix A, Fig. 4a, Appendix B, Fig. S5), equation (2) can be approximated by

$$Ras = \frac{1}{1 + pKe}. \qquad (2')$$

This approximation clearly highlights the characteristics of the *Ras* activation at steady state which becomes constant and independent of *pR* (Fig. 6f). The slope of the plot of the *Ras* activation, which corresponds to the order of the reactions from *pR* to the *Ras* activation, was lower than that of the *Rap1* activation under the conditions such as

$\alpha << 1$ and $p\alpha << 1$ (Fig. 6e, f), characterising the distinct dynamics between the *Ras* and *Rap1* activation at steady state.

Next, we confirmed that the simple Ras model represents the same characteristics as the transient Ras activation *in silico* (Appendix A). Responses of the transient Ras activation versus the indicated values of q and r *in silico* were very similar to those in the simple Ras model (Fig. 6b, c; Fig. 7a, b), where q, r and $Ras_{transient}$ denote the inverse number of the relative time constant of RasGAP, increasing rate of phosphorylated EGFR and the relative peak amplitude of the transient Ras activation, respectively (Appendix B, Fig. S5). These results indicate that the simple Ras model retains essential characteristics of the transient Ras activation *in silico*.

We also confirmed that the simple Rap1 and Ras models represent the same characteristics of the Rap1 and Ras activation at steady state *in silico*. We examined the Rap1 and Ras activation in dose-dependent manners in constant phosphorylated EGFR and TrkA. The slopes of the plot of the Rap1 activation versus both phosphorylated receptors at steady state were very similar at lower doses (Fig. 7c). The slopes of the plots of the Ras activation versus both phosphorylated receptors at steady state were also similar at lower doses (Fig. 7c). However, the slopes of the plots of the Ras activation were lower than those of the Rap1 activation at the lower doses, where the GEF and GAP activation were not saturated (Fig. 4a, b, Appendix A). This *in silico* characteristics is consistent with the result in the simple Rap1 and Ras models (Fig. 6e, f), indicating that the simple Rap1 and Ras models also retain essential characteristics of the Rap1 and Ras activation at steady state *in silico*. The inhibition of the Ras activation at higher doses of both phosphorylated receptors depended on the negative feedback inhibition of SOS; the deletion of the negative feedback inhibition of SOS

resulted in the disappearance of this inhibition at higher doses without affecting Ras activation at lower doses (Fig. 7c). It is also possible that the negative feedback inhibition of SOS regulates the Ras activation even at lower doses *in vivo*, and further study is necessary to address this issue.

We also predicted the dynamics of the ERK activation at steady state against the phosphorylated receptors *in silico*. The slope of the plot of the ERK activation versus the phosphorylated EGFR at steady state was lower than that versus the phosphorylated TrkA (Fig. 7d). The ERK activation at steady state consisted of the Ras- (Fig. 7d, dotted lines) and Rap1-dependent (Fig. 7d, dashed line) ERK activation *in silico*. The Ras-dependent ERK activation became dominant at lower doses of the phosphorylated receptors, below the intersecting points (Fig. 7d). In turn, the Rap1-dependent ERK activation became dominant at higher doses of the phosphorylated receptors, above the intersecting points (Fig. 7d). The curves of the Ras-dependent ERK activation were similar, whereas those of the Rap1-dependent ERK activation were different, leading to different slopes of the ERK activation versus both phosphorylated receptors. The distinct Rap1 activation against both phosphorylated receptors is due to the distinct affinities of FRS2 to both receptors (see below).

Based on this *in silico* prediction, we attempted to validate the distinct properties of the sustained ERK activation *in vivo*. We examined the sustained ERK activation versus the sustained phosphorylated EGFR and TrkA *in vivo*. The slope of the plot of the ERK activation versus the phosphorylated EGFR was lower than that versus the phosphorylated TrkA (Fig. 7e, f), which is consistent with the *in silico* prediction. Thus, these *in silico* and *in vivo* results clearly indicate the distinct dynamics of the ERK

activation against the phosphorylated EGFR and TrkA at steady state.

2. Discussion and Conclusions

The dynamics of adaptor proteins and receptors are responsible for the difference between EGF- and NGF-dependent sustained ERK activation

The critical difference between EGF- and NGF-dependent ERK activation is the absence or presence of the sustained ERK activation which depends on the sustained Rap1 activation. What is the origin of this difference? In this model, one of the most critical differences came from the different affinities of FRS2 for the phosphorylated receptors. The affinity of FRS2 for phosphorylated TrkA was higher than that for phosphorylated EGFR (Table S1). Reduction of the affinity of FRS2 for phosphorylated TrkA reduced the sustained Rap1 activation (Fig. S3), indicating that the sustained Rap1 activation depends on the affinity of FRS2 for phosphorylated TrkA. The amplitude of the Rap1 activation in response to NGF became similar to that in response to EGF when the affinities of FRS2 for both phosphorylated receptors were set at 200 nM (Fig. S3, solid and dashed green lines), indicating that the affinity of FRS2 for the phosphorylated receptor determines the amplitude of the Rap1 activation. Another critical difference was the different dynamics of tyrosine phosphorylation of the receptors. NGF induced the sustained tyrosine phosphorylation of TrkA (Fig. 1c), whereas EGF induced the transient tyrosine phosphorylation of EGFR due to the rapid internalisation and degradation (Figs. 1b, 5c). Furthermore, from downstream of the adaptor proteins to ERK, both the topology of the network and kinetic parameters are identical regardless of the stimuli, indicating that the difference of the EGF- and NGF-

dependent ERK activation is due to the different dynamics upstream of the adaptor proteins. Thus, the different dynamics of the adaptor proteins and the receptor tyrosine phosphorylation are the main origins of the difference of the EGF- and NGF-dependent sustained Rap1 activation, as well as the distinct dynamics of the sustained ERK activation in response to the sustained phosphorylated EGF and TrkA (Fig. 7d-f).

Possible physiological roles of the distinct temporal dynamics of transient and sustained ERK activation

Members of the EGF family are evolutionarily conserved morphogens that affect traits from vulva formation in *Caenorhabditis elegans* (Katz et al., 1995), eye development (Freeman, 1997) and leg pattern formation (Campbell, 2002) in *Drosophila*, and epithelial development in mammals. Spatial gradient of the EGF family is critical for these developmental processes, indicating that the concentration-dependent effect of the EGF family is critical for such processes. Because the spatial gradient should accompany some temporal patterns, temporal and spatial gradients of the EGF family may distinctly use the distinct temporal dynamics of the transient and sustained ERK activation at specific cell positions in such developmental processes.

Several members of the EGF family, including heparin-binding EGF-like growth factor (HB-EGF) act as membrane-anchored form, or the soluble form released by ectodomain shedding, which inhibits and stimulates cell growth, respectively (Iwamoto and Mekada, 2000). The soluble form and the membrane-anchored form of the EGF family may induce transient and sustained tyrosine phosphorylation of EGFR, respectively. EGFR bound to the soluble form may be rapidly internalised and degraded, resulting in the transient stimulation of the receptors, whereas the EGFR

bound to the membrane-anchored form of the EGF family may be prevented from internalisation, resulting in the sustained stimulation. Similarly in PC12 cells, the sustained EGFR stimulation using immobilised EGF resulted in the sustained ERK activation and subsequent differentiation (Ito et al., 2001). Taken together with our results, we propose that the soluble form of the EGF family induces rapid stimulation of the receptor and thereby induces temporal rate-dependent ERK activation, whereas the membrane-anchored form induces sustained receptor stimulation and thereby induces concentration-dependent ERK activation.

Our results raise another interesting possibility: under physiological conditions, EGF should act rapidly, whereas NGF can act slowly. If this is the case, physiological NGF-dependent ERK activation might not require the transient Ras activation; we found that the slow NGF stimulus did not induce the transient Ras activation *in silico* (Fig. 4a). Thus, experiments that use constant stimulation require careful quantitative interpretation, because constant stimulation might induce the activation of a certain molecule(s) that is not physiologically used by slow stimuli.

Various mechanisms of sustained ERK activation

Sustained ERK activation has been observed in various cell lines including NIH 3T3 cells in response to EGF (Stork and Schmitt, 2002) and in progesterone-dependent *Xenopus* oogenesis (Xiong and Ferrell, 2003). The sustained ERK activation can be achieved by various mechanisms. For example, slower EGFR internalisation can induce the sustained ERK activation (Fig. 5c), consistent with the observation of the sustained ERK activation using immobilised EGF in PC12 cells (Ito et al., 2001). Also, lower expression levels of RasGAP (Fig. 5b) or Dok can lead to the similar sustained

ERK activation. Slower dephosphorylation of ERK has been proposed to be responsible for the EGF-dependent sustained ERK activation in the *in silico* models (Schoeberl et al., 2002). However, in PC 12 cells, the slower dephosphorylation of ERK is unlikely to be involved in the EGF-dependent ERK activation because EGF only induced the transient ERK activation (Fig. 1h). The sustained ERK activation in *Xenopus* oocytes (Xiong and Ferrell, 2003) and NIH3T3 cells (Bhalla et al., 2002) is mediated by a positive feedback loop. In these cells, a clear bistability of ERK activation was observed in the sustained phase. In contrast to these cells, we did not observe a clear bistability of the sustained ERK activation in individual PC12 cells (data not shown).

In a previous NGF-dependent ERK activation model (Brightman and Fell, 2000), the sustained Ras activation was responsible for the sustained ERK activation. However, the sustained Ras activation is unlikely to explain the sustained ERK activation because NGF induced only transient Ras activation in PC12 cells (Kao et al., 2001; Wu et al., 2001) (Fig. 1e). Therefore, it is likely that, in PC12 cells, the NGF-dependent sustained ERK activation depends on the sustained Rap1 activation mediated by the sustained tyrosine phosphorylation of TrkA rather than a positive feedback loop or the sustained Ras activation. In addition, these above mechanisms may explain why EGF induces the sustained ERK activation in some cell lines and the transient ERK activation in other cell lines, including PC12 cells.

We showed that the temporal rate and final concentration of growth factors are specifically captured by the Ras and Rap1 systems via the transient Ras and sustained Rap1 activation, and then encoded into the transient and sustained ERK activation, respectively (Fig. 8). This difference between the Ras and Rap1 systems came from

their distinct inactivation processes; slower and constant GAP activity, respectively. These results highlight a novel general aspect of signalling mechanisms — slow feedforward inhibition can make the molecular system capture the temporal rate of stimulation — as well as the possible physiological roles of stimulation-dependent negative regulators (Moghal and Sternberg, 1999) such as other GAPs (e.g.,RhoGAP), protein tyrosine phosphatases (e.g., SHP), and lipid phosphatases (e.g., SHIP and PTEN) in capturing the temporal rate of stimulation. Although physiological roles of transient activation of downstream molecules including that of ERK remain to be elucidated, the fact that there are many signalling systems with a feedforward inhibition implies a possibility that rapid, but not slow, stimulation is specifically used for some biological processes. Further study is necessary to address this issue.

Transient and sustained ERK activation distinctly regulate protein expression levels of immediate early genes such as c-*fos* via stabilisation of the protein (Murphy et al., 2002). The downstream signalling networks including genes and proteins expression of immediate early genes can be readily incorporated into this *in silico* model, which will provide us the first integrated biochemical model of the effects of growth factors on genes and protein expression.

Methodological concerns and suggestions for further research

We should emphasise that the current *in silico* model does not exclude the possibility that additional unknown networks are needed. Furthermore, each *in silico* network should be regarded as representative of similar redundant processes, rather than as a complete description. For example, FRS2 is only an adaptor protein for the Rap1

activation in the current *in silico* model; however, this protein implicitly represents another adaptor protein, ARMS which performs a similar function (Arevalo et al., 2004).

In this thesis, we applied a combined approach of *in silico* and *in vivo* analysis to understand ERK signaling network as a system. The key procedure of this approach is the construction of an *in silico* model. As shown in the previous chapter, *in vivo* dynamics has been successfully reproduced *in silico* by fitting the *in silico* parameter manually on the basis of *in vivo* dynamics and kinetic parameter reported in the literature. As long as the complexity dose not exceed our current model, we can determine appropriate parameters, which can be considered as within the physiological range, on the basis of biological knowledge and experience. Although biologists will recognize the similarity between *in vivo* and *in silico* dynamics by their experience and intuition, a quantitative measure of similarity must be introduced to evaluate the likelihood of different models. Furthermore, by employing efficient parameter fitting methods provided by recent intensive bioinformatics studies (Sachs et al., 2005) will evolve our approach into a mature methodology.

In this thesis, the validation of the *in silico* model has been performed by comparing *in vivo* and *in silico* dynamics in response to various patterns of stimulation, which extrapolate given conditions used for the construction of the model. Thus, the conditions that extrapolate the model can be used to validate the model, and to further improve the model if some discrepancies were found. In light of this, we suggest an additional methodological strategy that can be used to develop and refine a more convincing *in silico* model. For example, this methodology can be applied to our constructed *in silico* model to explain distinct ERK dynamics seen in the different cell lines of PC12 cells or in other cell lines that were derived from different organs.

Among the parameters in the model, kinetic constants such as forward and backward reaction constants will be same in all these cell lines, as long as they are derived from a single species. On the other hand, it is surmised that expression level of molecules changes greatly with cell lines. Accordingly, the difference in the ERK dynamics should be explained by the difference in the expression level of molecules, and other additional networks that we could disregard due to the negligible expression level of certain molecules. Therefore, constraining kinetic parameters by *in vivo* dynamics observed in different cell lines is an efficient way to estimate and validate an *in silico* model without increase in the complexity of the model. In this case, however, an automated parameter fitting method must exist to satisfy all conditions due to the increasing restraint on the model.

Conclusion

Constraining *in silico* dynamics of the cross-talk points of the signalling networks by *in vivo* dynamics allowed us to generate a highly predictive model, and the *in silico* prediction of the hidden properties of signalling networks can be further validated by measuring *in vivo* dynamics. Thus, combining *in silico* and *in vivo* analyses facilitates systematic understanding of the underlying properties of signalling networks.

Methods

Numerical simulation of biochemical reactions

All reactions were represented by molecule-molecule interactions and enzymatic reactions. A molecule-molecule interaction is described by the following formula:

$$\mathrm{A} + \mathrm{B} \underset{k_b}{\overset{k_f}{\rightleftarrows}} \mathrm{AB},$$

where k_f and k_b are the rate constants for the forward and backward reactions, respectively. Dissociation constant, *K*d, is defined as $K\mathrm{d} = k_b / k_f$. For calculation of the AB complex, the above reaction is represented as a differential equation of the form,

$$d[\mathrm{AB}]/dt = k_f[\mathrm{A}][\mathrm{B}] - k_b[\mathrm{AB}]$$

where [A], [B] and [AB] denote the concentrations of A, B and AB, respectively.

An enzymatic reaction is described as the following Michaelis-Menten formula:

$$\mathrm{S} + \mathrm{E} \underset{k_{-1}}{\overset{k_1}{\rightleftarrows}} \mathrm{SE} \xrightarrow{k_{cat}} \mathrm{P} + \mathrm{E},$$

where S, E and P denote a substrate, an enzyme, and a product, respectively. The Michaelis constant, *K*m, is defined as $K\mathrm{m} = (k_{-1} + k_{cat}) / k_1$. The maximum enzyme velocity, $V_{\max}$, is defined as $V_{\max} = k_{cat}[\mathrm{E}]_{\mathrm{total}}$, where $[\mathrm{E}]_{\mathrm{total}}$ is the total concentration of the enzyme. We used a *GENESIS* simulator (version 2.2) with a *Kinetikit* interface for solving the ordinary differential equations with a time step of 10 ms (Bhalla and Iyengar, 1999).

Block diagram and parameters

The model consisted of 22 molecules and 106 rate constants. The rate constants consisted of 70 and 36 rate constants for molecule-molecule interactions and enzymatic

reactions, respectively. The biochemical reactions and the rate constants used in the study are shown in Appendix B, Figure S1 and Table S1, respectively. The *GENESIS* script of our *in silico* model is also available as a text file on our website (http://www.kurodalab.org/info/ERK.g).

Cell culture and growth factor treatments

PC12 cells (kindly provided by Masato Nakafuku, Cincinnati Children's Hospital Medical Center) were grown in Dulbecco's modified Eagle's medium (DMEM) (Sigma, St. Louis, MO) supplemented with 10% foetal bovine serum (ThermoTrace, Melbourne, Australia) and 5% horse serum (JRH, Biosciences, Lenexa, KS), and were maintained at 37 °C in a saturating humidified atmosphere of 95% air and 5% CO_2. Cells (8×10^5) were starved in DMEM for 16 h, then stimulated with the indicated concentrations of NGF (Invitrogen, Carlsbad, CA) or EGF (Roche, Indianapolis, IN). Increasing stimuli of EGF and NGF were added by use of a microsyringe pump (KD Scientific, Holliston, MA) with continuous 10 μl/min flow rate into 2 ml of the cultured media. After the addition of ice-cold 10% trichloroacetic acid with 10mM dithiothreitol (DTT), cells were precipitated by centrifuge at 20,000 x *g* at 4°C for 10 min. Pellets were washed with acetone with 10mM DTT and dissolved in sodium dodecyl sulfate-polyacrylamide gel electrophoresis (SDS-PAGE) sample buffer.

Immunoblotting

Cell lysates were subjected to standard SDS-PAGE (acrylamide:bis=29.5:1) or low-bis SDS-PAGE (acrylamide:bis=144:1) for the separation of phosphorylated and nonphosphorylated ERK, and transferred to nitrocellulose membrane. The membranes

were probed with anti-phospho EGFR (Y1068) antibody (1:1,000, Cell Signaling Technology, Beverly, MA), anti-phospho TrkA (Y490) antibody (1:1,000, Cell Signaling Technology), anti-SOS1 antibody (1:1,000, Upstate, Charlottesville, VA), or anti-ERK1/2 antibody (1:1,000, Cell Signaling Technology). Anti-phospho ERK1/2 (T202/Y204) antibody (1:1000, Cell Signaling Technology) was used because of the higher sensitivity compared to that of anti-ERK1/2 antibody, and the ratio between phosphorylated and non-phosphorylated ERK2 were estimated by the comparison with the same point (5 ng/ml NGF) using anti-ERK1/2 antibody (Fig. 7e, f). Horseradish peroxidase (HRP) conjugated secondary antibodies (Amersham Biosciences) were used at 1:5,000 and an enhanced-chemiluminescence (ECL) detection kit (Amersham Biosciences, Piscataway, NJ) was used for HRP detection. Chemiluminescent signals were captured with LightCapture system (ATTO, Tokyo, Japan) and quantified by CS analyser software (ATTO).

Ras and Rap1 pulldown assay

Ras and Rap1 activation was measured by an affinity pulldown assay as described elsewhere (de Rooij and Bos, 1997). Essentially, after NGF or EGF stimulation, cells were washed with ice-cold phosphate-buffered saline and lysed with lysis buffer (10% glycerol, 1% Nonidet P-40, 50 mM Tris [pH 7.4], 20 mM NaCl, 2.5 mM $MgCl_2$, 10 μg/ml leupeptin, 10 μg/ml aprotinin, 1 mM phenylmethysulfonyl fluoride, 10 mM NaF and 1 mM Na_3VO_4). Cell lysates were centrifuged for 5 min at 20,000 x *g* and the supernatants were incubated for 1 h at 4°C with GST-c-Raf1 (1 – 149 amino acids) or GST-RalGDS (767 – 867 amino acids) (kindly provided by Akira Kikuchi, Hiroshima University, Japan) coupled glutathione-sepharose beads to isolate activated Ras or Rap1,

respectively. After washing with ice-cold lysis buffer three times, the small GTPases bound to the beads were eluted by SDS-PAGE sample buffer and subjected to SDS-PAGE, followed by immunoblotting with monoclonal anti-Ras (1:500, BD biosciences, Franklin Lakes, NJ) or anti- Rap1 (1:500, BD biosciences) antibodies.

Recruitment of SOS and RasGAP to the membrane fractions

PC12 cells were stimulated with a constant 10 ng/ml of EGF, and cells were lysed by sonication at the indicated time with the buffer containing 50 mM Tris [pH 7.5], 200 mM sucrose, 2.5 mM $MgCl_2$, 10 mM NaF, 1 mM sodium orthovanadate, 1 mM dithiothreitol and 10 μg/ml leupeptin and aprotinin. After the membrane and cytosol fractions were separated by the centrifugation at 100,000 x *g* for 30 min, the amounts of SOS and RasGAP in both fractions were measured by western blotting.

References

Arevalo, J.C., H. Yano, K.K. Teng, and M.V. Chao. 2004. A unique pathway for sustained neurotrophin signaling through an ankyrin-rich membrane-spanning protein. *EMBO J.* 23:2358-2368.

Bhalla, U.S., and R. Iyengar. 1999. Emergent properties of networks of biological signaling pathways. *Science*. 283:381-387.

Bhalla, U.S., P.T. Ram, and R. Iyengar. 2002. MAP kinase phosphatase as a locus of flexibility in a mitogen-activated protein kinase signaling network. *Science*. 297:1018-1023.

Bourne, H.R., D.A. Sanders, and F. McCormick. 1991. The GTPase superfamily: conserved structure and molecular mechanism. *Nature*. 349:117-127.

Brightman, F.A., and D.A. Fell. 2000. Differential feedback regulation of the MAPK cascade underlies the quantitative differences in EGF and NGF signalling in PC12 cells. *FEBS Lett.* 482:169-174.

Bruggeman, F.J., H.V. Westerhoff, J.B. Hoek, and B.N. Kholodenko. 2002. Modular response analysis of cellular regulatory networks. *J. Theor. Biol.* 218:507-520.

Campbell, G. 2002. Distalization of the Drosophila leg by graded EGF-receptor activity. *Nature*. 418:781-785.

Chang, J.H., E. Mellon, N.C. Schanen, and J.L. Twiss. 2003. Persistent TrkA activity is necessary to maintain transcription in neuronally differentiated PC12 cells. *J. Biol. Chem.* 278:42877-42885.

Choi, D.Y., J.J. Toledo-Aral, R. Segal, and S. Halegoua. 2001. Sustained signaling by phospholipase C-gamma mediates nerve growth factor-triggered gene expression. *Mol. Cell. Biol.* 21:2695-2705.

Davis, R.J. 1993. The mitogen-activated protein kinase signal transduction pathway. *J. Biol. Chem.* 268:14553-14556.

de Rooij, J., and J.L. Bos. 1997. Minimal Ras-binding domain of Raf1 can be used as an activation-specific probe for Ras. *Oncogene*. 14:623-5.

Di Fiore, P.P., and G.N. Gill. 1999. Endocytosis and mitogenic signaling. *Curr. Opin. Cell. Biol.* 11:483-488.

Dong, C., S.B. Waters, K.H. Holt, and J.E. Pessin. 1996. SOS phosphorylation and disassociation of the Grb2-SOS complex by the ERK and JNK signaling pathways. *J. Biol. Chem.* 271:6328-6332.

Downward, J. 1994. The GRB2/Sem-5 adaptor protein. *FEBS Lett.* 338:113-117.

Egan, S.E., B.W. Giddings, M.W. Brooks, L. Buday, A.M. Sizeland, and R.A. Weinberg. 1993. Association of Sos Ras exchange protein with Grb2 is implicated in tyrosine kinase signal transduction and transformation. *Nature*. 363:45-51.

Freeman, M. 1997. Cell determination strategies in the Drosophila eye. *Development*. 124:261-270.

Gale, N.W., S. Kaplan, E.J. Lowenstein, J. Schlessinger, and D. Bar-Sagi. 1993. Grb2 mediates the EGF-dependent activation of guanine nucleotide exchange on Ras. *Nature*. 363:88-92.

Gotoh, Y., E. Nishida, T. Yamashita, M. Hoshi, M. Kawakami, and H. Sakai. 1990. Microtubule-associated-protein (MAP) kinase activated by nerve growth factor and epidermal growth factor in PC12 cells. Identity with the mitogen-activated MAP kinase of fibroblastic cells. *Eur. J. Biochem.* 193:661-669.

Hatakeyama, M., S. Kimura, T. Naka, T. Kawasaki, N. Yumoto, M. Ichikawa, J.H. Kim, K. Saito, M. Saeki, M. Shirouzu, S. Yokoyama, and A. Konagaya. 2003. A computational model on the modulation of mitogen-activated protein kinase (MAPK) and Akt pathways in heregulin-induced ErbB signalling. *Biochem. J.* 373:451-463.

Heinrich, R., B.G. Neel, and T.A. Rapoport. 2002. Mathematical models of protein kinase signal transduction. *Mol. Cell*. 9:957-970.

Holt, K.H., S.B. Waters, S. Okada, K. Yamauchi, S.J. Decker, A.R. Saltiel, D.G. Motto, G.A. Koretzky, and J.E. Pessin. 1996. Epidermal growth factor receptor targeting prevents uncoupling of the Grb2-SOS complex. *J. Biol. Chem.* 271:8300-8306.

Ito, Y., G. Chen, Y. Imanishi, T. Morooka, E. Nishida, Y. Okabayashi, and M. Kasuga. 2001. Differential control of cellular gene expression by diffusible and non-diffusible EGF. *J. Biochem. (Tokyo)*. 129:733-737.

Iwamoto, R., and E. Mekada. 2000. Heparin-binding EGF-like growth factor: a juxtacrine growth factor. *Cytokine Growth Factor Rev.* 11:335-344.

Jones, N., and D.J. Dumont. 1999. Recruitment of Dok-R to the EGF receptor through its PTB domain is required for attenuation of Erk MAP kinase activation. *Curr. Biol.* 9:1057-1060.

Kao, S., R.K. Jaiswal, W. Kolch, and G.E. Landreth. 2001. Identification of the mechanisms regulating the differential activation of the mapk cascade by epidermal growth factor and nerve growth factor in PC12 cells. *J. Biol. Chem.* 276:18169-18177.

Katz, W.S., R.J. Hill, T.R. Clandinin, and P.W. Sternberg. 1995. Different levels of the C. elegans growth factor LIN-3 promote distinct vulval precursor fates. *Cell*. 82:297-307.

Kholodenko, B.N., O.V. Demin, G. Moehren, and J.B. Hoek. 1999. Quantification of short term signaling by the epidermal growth factor receptor. *J. Biol. Chem.* 274:30169-30181.

Langlois, W.J., T. Sasaoka, A.R. Saltiel, and J.M. Olefsky. 1995. Negative feedback regulation and desensitization of insulin- and epidermal growth factor-stimulated p21ras activation. *J. Biol. Chem.* 270:25320-25323.

Li, N., A. Batzer, R. Daly, V. Yajnik, E. Skolnik, P. Chardin, D. Bar-Sagi, B. Margolis, and J. Schlessinger. 1993. Guanine-nucleotide-releasing factor hSos1 binds to Grb2 and links receptor tyrosine kinases to Ras signalling. *Nature*. 363:85-88.

Longva, K.E., F.D. Blystad, E. Stang, A.M. Larsen, L.E. Johannessen, and I.H. Madshus. 2002. Ubiquitination and proteasomal activity is required for transport of the EGF receptor to inner membranes of multivesicular bodies. *J. Cell Biol.* 156:843-854.

Marshall, C.J. 1998. Signal transduction. Taking the Rap. *Nature*. 392:553-554.

Moghal, N., and P.W. Sternberg. 1999. Multiple positive and negative regulators of signaling by the EGF-receptor. *Curr. Opin. Cell Biol.* 11:190-196.

Murphy, L.O., S. Smith, R.H. Chen, D.C. Fingar, and J. Blenis. 2002. Molecular interpretation of ERK signal duration by immediate early gene products. *Nat. Cell Biol.* 4:556-564.

Nishida, E., and Y. Gotoh. 1993. The MAP kinase cascade is essential for diverse signal transduction pathways. *Trends Biochem. Sci.* 18:128-131.

Ohtsuka, T., K. Shimizu, B. Yamamori, S. Kuroda, and Y. Takai. 1996. Activation of brain B-Raf protein kinase by Rap1B small GTP-binding protein. *J. Biol. Chem.* 271:1258-1261.

Qiu, M.S., and S.H. Green. 1992. PC12 cell neuronal differentiation is associated with prolonged p21ras activity and consequent prolonged ERK activity. *Neuron*. 9:705-717.

Rozakis-Adcock, M., R. Fernley, J. Wade, T. Pawson, and D. Bowtell. 1993. The SH2 and SH3 domains of mammalian Grb2 couple the EGF receptor to the Ras activator mSos1. *Nature*. 363:83-85.

Sachs, K., O. Perez, D. Pe'er, D.A. Lauffenburger, and G.P. Nolan. 2005. Causal protein-signaling networks derived from multiparameter single-cell data. *Science*. 308:523-9.

Schoeberl, B., C. Eichler-Jonsson, E.D. Gilles, and G. Muller. 2002. Computational modeling of the dynamics of the MAP kinase cascade activated by surface and internalized EGF receptors. *Nat. Biotechnol.* 20:370-375.

Shvartsman, S.Y., M.P. Hagan, A. Yacoub, P. Dent, H.S. Wiley, and D.A. Lauffenburger. 2002. Autocrine loops with positive feedback enable context-dependent cell signaling. *Am. J. Physiol. Cell. Physiol.* 282:C545-559.

Soler, C., L. Beguinot, A. Sorkin, and G. Carpenter. 1993. Tyrosine phosphorylation of ras GTPase-activating protein does not require association with the epidermal growth factor receptor. *J. Biol. Chem.* 268:22010-22019.

Stork, P.J., and J.M. Schmitt. 2002. Crosstalk between cAMP and MAP kinase signaling in the regulation of cell proliferation. *Trends Cell Biol.* 12:258-266.

Traverse, S., N. Gomez, H. Paterson, C. Marshall, and P. Cohen. 1992. Sustained activation of the mitogen-activated protein (MAP) kinase cascade may be required for differentiation of PC12 cells. Comparison of the effects of nerve growth factor and epidermal growth factor. *Biochem. J.* 288 (Pt 2):351-355.

Vaudry, D., P.J. Stork, P. Lazarovici, and L.E. Eiden. 2002. Signaling pathways for PC12 cell differentiation: making the right connections. *Science*. 296:1648-1649.

Vossler, M.R., H. Yao, R.D. York, M.G. Pan, C.S. Rim, and P.J. Stork. 1997. cAMP activates MAP kinase and Elk-1 through a B-Raf- and Rap1-dependent pathway. *Cell*. 89:73-82.

Waterman, H., and Y. Yarden. 2001. Molecular mechanisms underlying endocytosis and sorting of ErbB receptor tyrosine kinases. *FEBS Lett.* 490:142-152.

Waters, S.B., K.H. Holt, S.E. Ross, L.J. Syu, K.L. Guan, A.R. Saltiel, G.A. Koretzky, and J.E. Pessin. 1995. Desensitization of Ras activation by a feedback disassociation of the SOS-Grb2 complex. *J. Biol. Chem.* 270:20883-20886.

Wu, C., C.F. Lai, and W.C. Mobley. 2001. Nerve growth factor activates persistent Rap1 signaling in endosomes. *J. Neurosci.* 21:5406-5416.

Xiong, W., and J.E. Ferrell, Jr. 2003. A positive-feedback-based bistable 'memory module' that governs a cell fate decision. *Nature*. 426:460-465.

Yamada, S., T. Taketomi, and A. Yoshimura. 2004. Model analysis of difference between EGF pathway and FGF pathway. *Biochem. Biophys. Res. Commun.* 314:1113-1120.

York, R.D., H. Yao, T. Dillon, C.L. Ellig, S.P. Eckert, E.W. McCleskey, and P.J. Stork. 1998. Rap1 mediates sustained MAP kinase activation induced by nerve growth factor. *Nature*. 392:622-666.

Figures

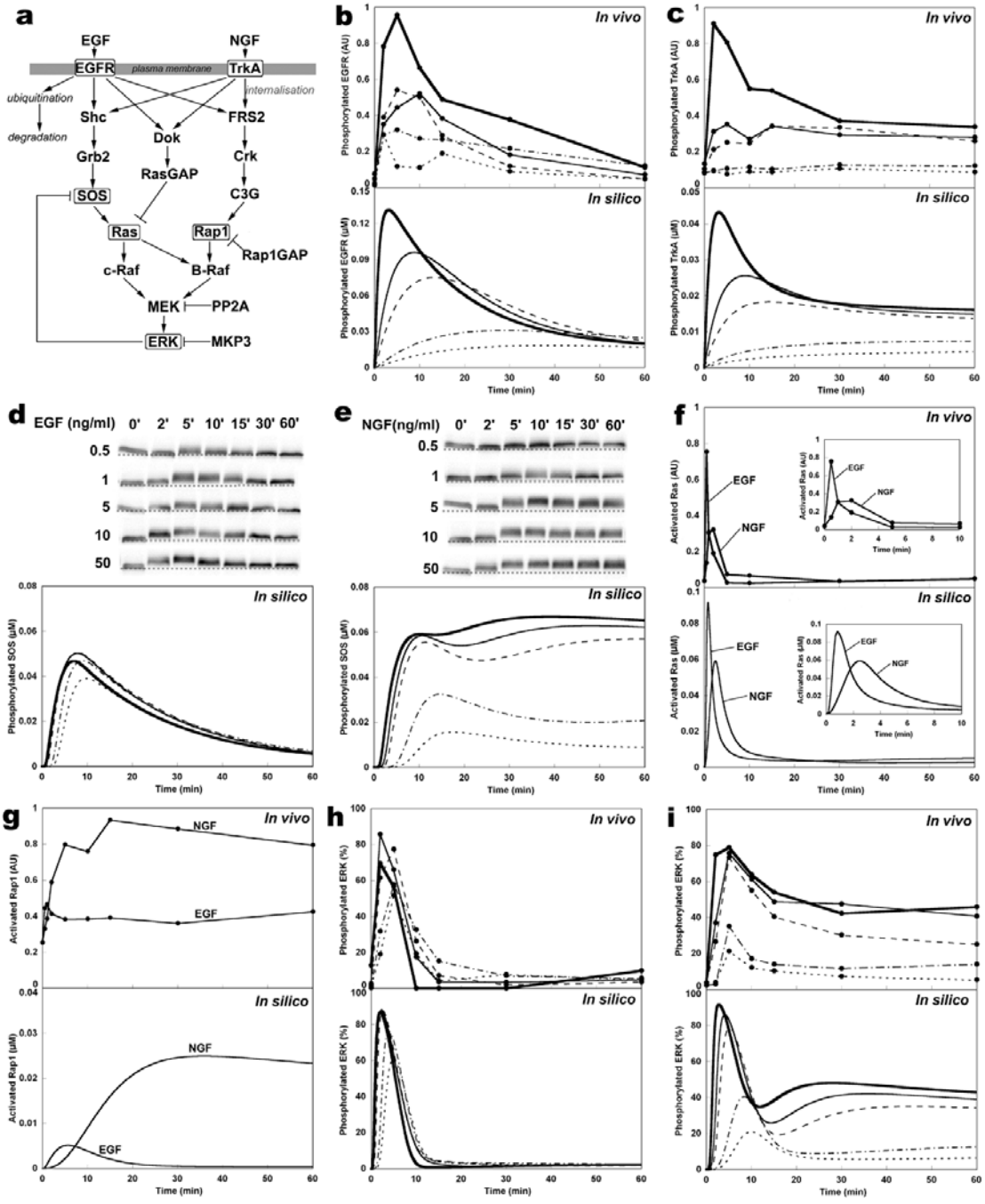

Figure 1 *In vivo* and *in silico* dynamics of ERK signalling networks. (**a**) Schematic overview of EGF- and NGF-dependent ERK signalling networks. Arrows and bars indicate stimulatory and inhibitory interactions, respectively. *In vivo* and *in silico* dynamics of cross-talk points were measured (**boxes**). Abbreviations: PP2A, protein phosphatase 2A; MKP3, MAP kinase

phosphatase 3. All the biochemical reactions and parameters are provided in the Appendix B, Figure S1 and Table S1, respectively. *In vivo* (**upper panel**) and *in silico* (**lower panel**) tyrosine phosphorylation of EGFR (**b**) and TrkA (**c**), EGF- (**d**) and NGF-dependent (**e**) phosphorylation of SOS, activation of Ras (**f**) and Rap1 (**g**), and EGF- (**h**) and NGF-dependent (**i**) phosphorylation of ERK. Dashed lines in the upper panels of **d** and **e** indicate the position of SOS at the basal level. Insets in **f** are the transient Ras activation within 10 min after stimulation. The thick line, thin line, thin dashed line, thin dash-dotted line, and thin dotted line indicate the responses with constant 50, 10, 5, 1 and 0.5 ng/ml of either EGF or NGF, respectively, except for Ras and Rap1 activation. For the Ras and Rap1 activation, 10 ng/ml of EGF or NGF was used. AU, arbitrary unit. The results are representative of three independent experiments. Images of the original gels of the western blotting (**b**-**i**) are shown in Figure S2.

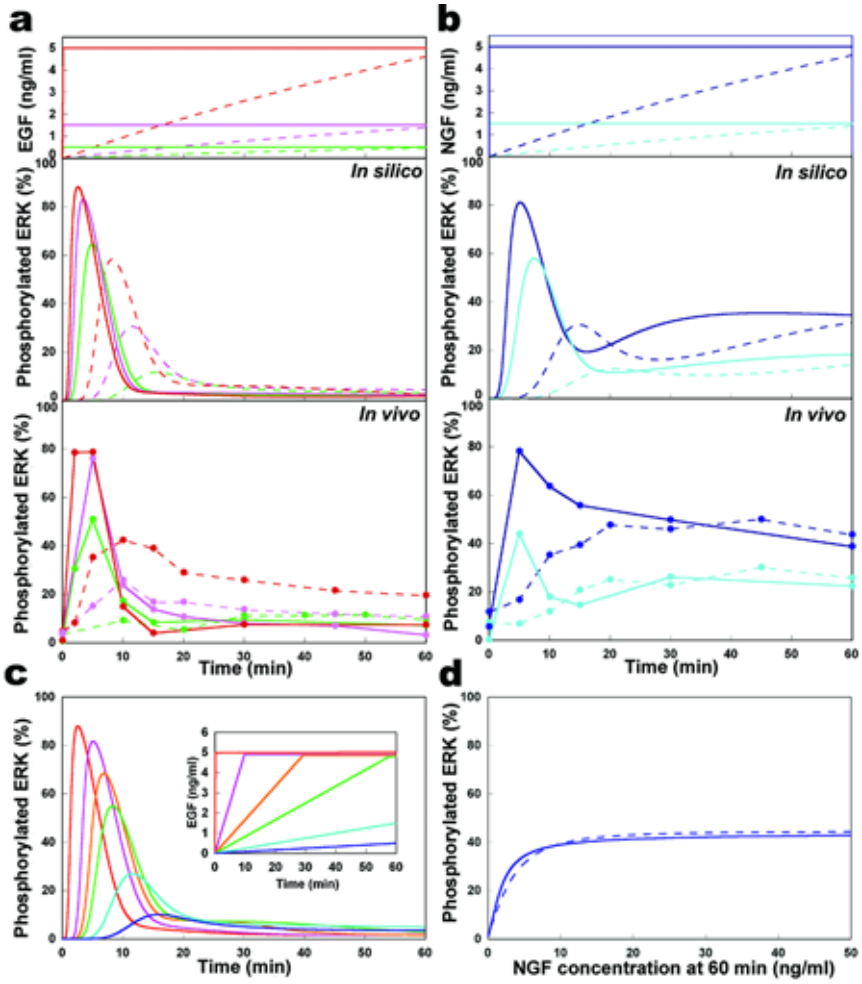

Figure 2 Distinct dynamics of transient and sustained ERK activation. For EGF (**a**) and NGF (**b**), the indicated stimuli (**upper panels**) were given and the ERK phosphorylation *in silico* (**middle panels**) and *in vivo* (**lower panels**) was plotted. The constant and increasing stimuli, and the corresponding responses are indicated by solid and dashed lines, respectively. The images of the original gels in **a** and **b** are shown in Fig. S2. (**c**) The temporal rate of EGF-dependent ERK phosphorylation *in silico*. The indicated EGF stimuli (inset) were given and the transient ERK activation was plotted. (**d**) The *in silico* sustained ERK phosphorylation at 60 min. Solid and dashed lines indicate the ERK phosphorylation at 60 min with constant and increasing NGF stimuli, respectively. The increasing stimuli are represented as the NGF concentrations at 60 min.

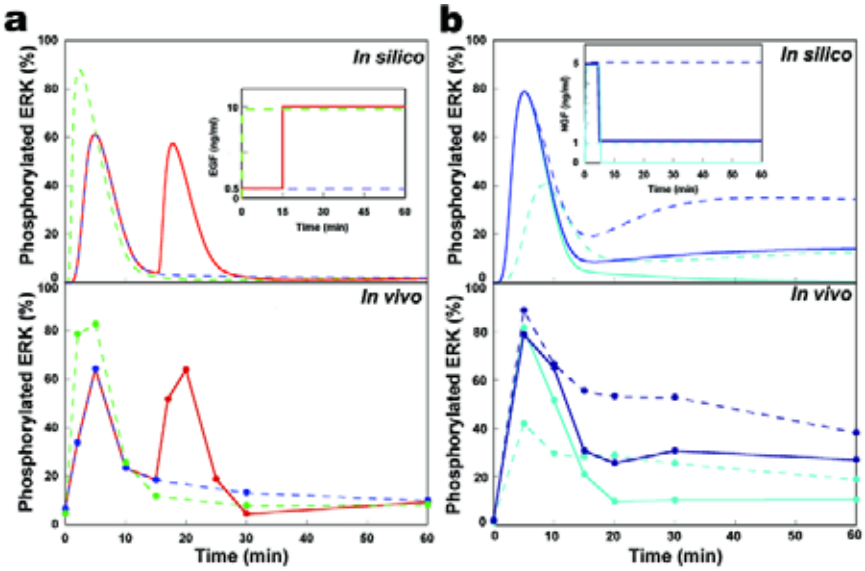

Figure 3 *In silico* and *in vivo* ERK activation in response to stepwise increases of EGF and to stepwise decreases of NGF. (**a**) The indicated stepwise increase of EGF stimulus (**inset**) was performed and ERK phosphorylation *in silico* (**upper panel**) and *in vivo* (**lower panel**) was plotted. The solid red line indicates the stepwise increases in EGF stimulus (0.5 to 10 ng/ml) and the corresponding ERK phosphorylation. The dashed blue and green lines indicate 0.5 and 10 ng/ml of constant EGF stimuli, respectively, and the corresponding ERK phosphorylation. (**b**) The indicated stepwise decrease of NGF or constant NGF stimulus (**inset**) was performed and ERK phosphorylation *in silico* (**upper panel**) and *in vivo* (**lower panel**) was plotted. The solid blue and cyan lines indicate the stepwise decreases of NGF stimuli (5 to 1 ng/ml and 5 to 0 ng/ml, respectively), and the corresponding ERK phosphorylation. The dashed blue and cyan lines indicate 5 and 1 ng/ml of constant NGF stimuli, respectively, and the corresponding ERK phosphorylation. The images of the original gels in **a** and **b** are shown in Fig. S2.

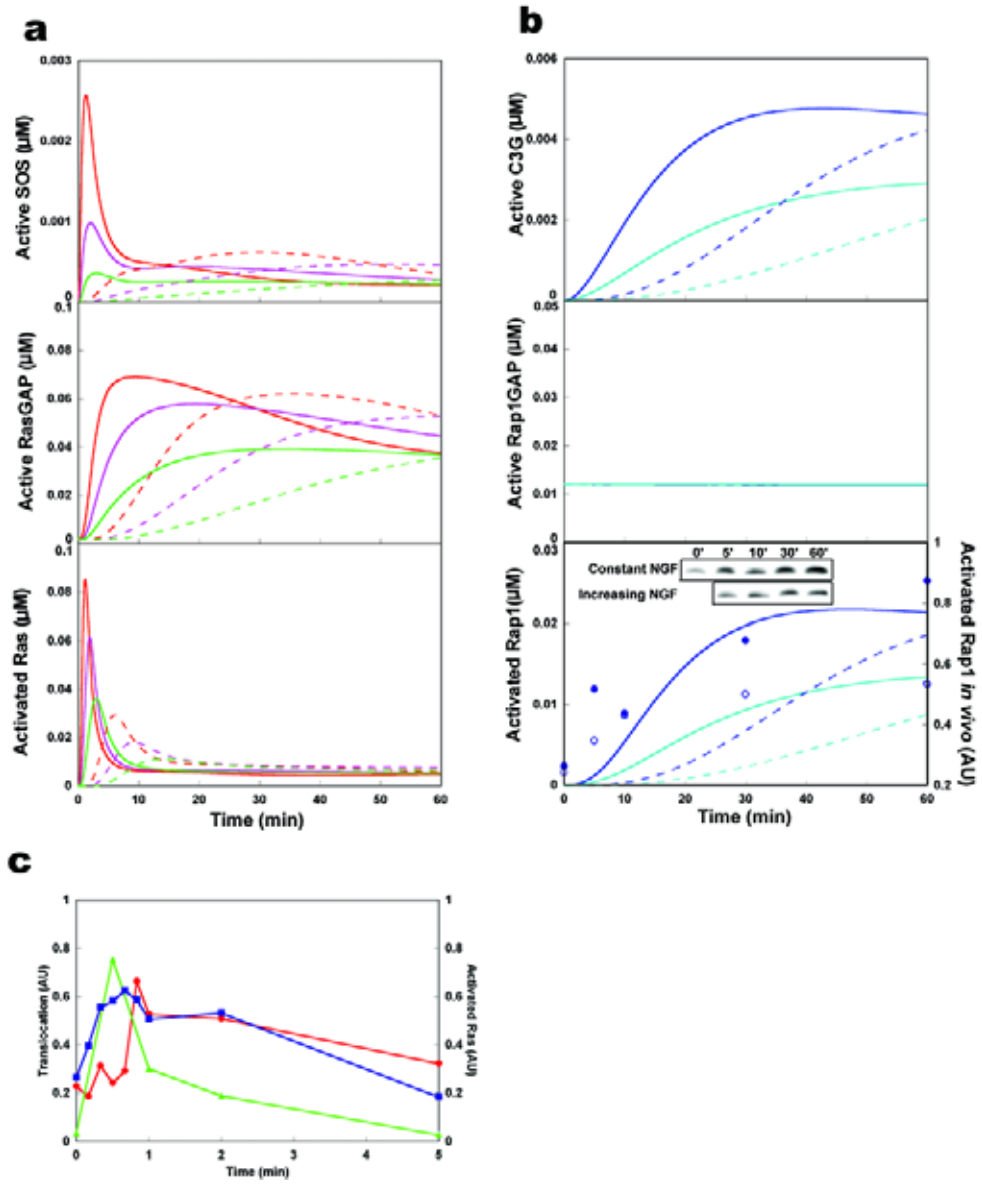

Figure 4 Distinct dynamics of EGF- and NGF-dependent Ras and Rap1 activation. The same stimuli as those shown in Figure 2 were given, and (**a**) the EGF-dependent active fractions of SOS (**upper panel**), RasGAP (**middle panel**) and Ras (**lower panel**), and (**b**) the NGF-dependent active fractions of C3G (**upper panel**), Rap1GAP (**middle panel**) and Rap1 (**lower panel**) were plotted *in silico* except that closed and open circles in **b** (**lower panel**) indicate the activated Rap1 *in vivo* in response to constant and increasing NGF stimuli (5 ng/ml at 60 min), respectively. Lines and colours are the same as in Figure 2.

Images of the original gels of the western blotting are shown in the inset. (**c**) *In vivo* recruitment of SOS and RasGAP to the membrane fraction in response to constant EGF stimulus. A constant EGF stimulus (10 ng/ml) was given, and the amounts of SOS (blue) and RasGAP (red) in the membrane fractions were measured. The *in vivo* activated Ras in Fig. 1f were also plotted (green). The images of the original gels in **c** are shown in Fig. S2.

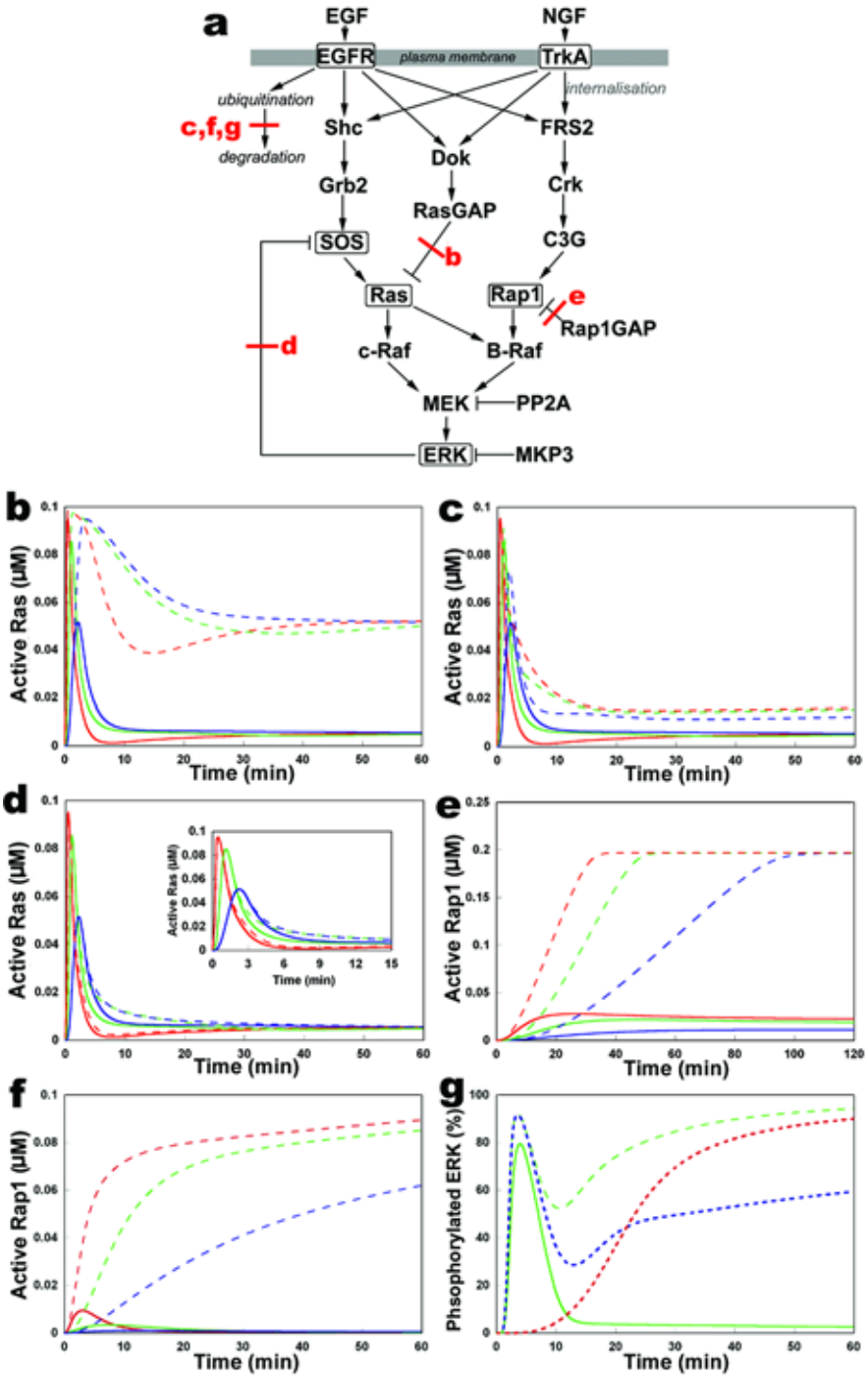

Figure 5 Roles of RasGAP, EGFR internalisation and ERK-dependent feedback inhibition of SOS, and Rap1GAP in Ras and Rap1 activation *in silico*. (**a**) The pathway indicated by a red bar was blocked and Ras and Rap1 activations were plotted as follows. Constant EGF stimuli were given in the presence or absence of either RasGAP (**b**), EGFR internalisation (**c, f**) and

ERK-dependent feedback inhibition of SOS (**d**), and Ras activation (**b**-**d**) and Rap1 activation (**f**) were plotted. Solid line, normal conditions; dashed line, in the absence of the indicated pathway. The inset in **d** is the transient Ras activation within 15 min after stimulation. (**e**) Constant NGF stimuli were given in the presence or absence of Rap1GAP, and Rap1 activation was plotted. Red, green and blue lines indicate the ERK phosphorylation with constant 50, 5 or 1 ng/ml of either EGF or NGF stimuli, respectively. (**g**) Constant EGF stimulus (1 ng/ml) was given in the presence or absence of EGFR internalisation, the Ras or the Rap1 activation, and the ERK activation were plotted. Green solid line, normal conditions; green dashed line, in the absence of EGFR internalisation; red dotted line, in the absence of EGFR internalisation and Ras activation; blue dotted line, in the absence of EGFR internalisation and Rap1 activation.

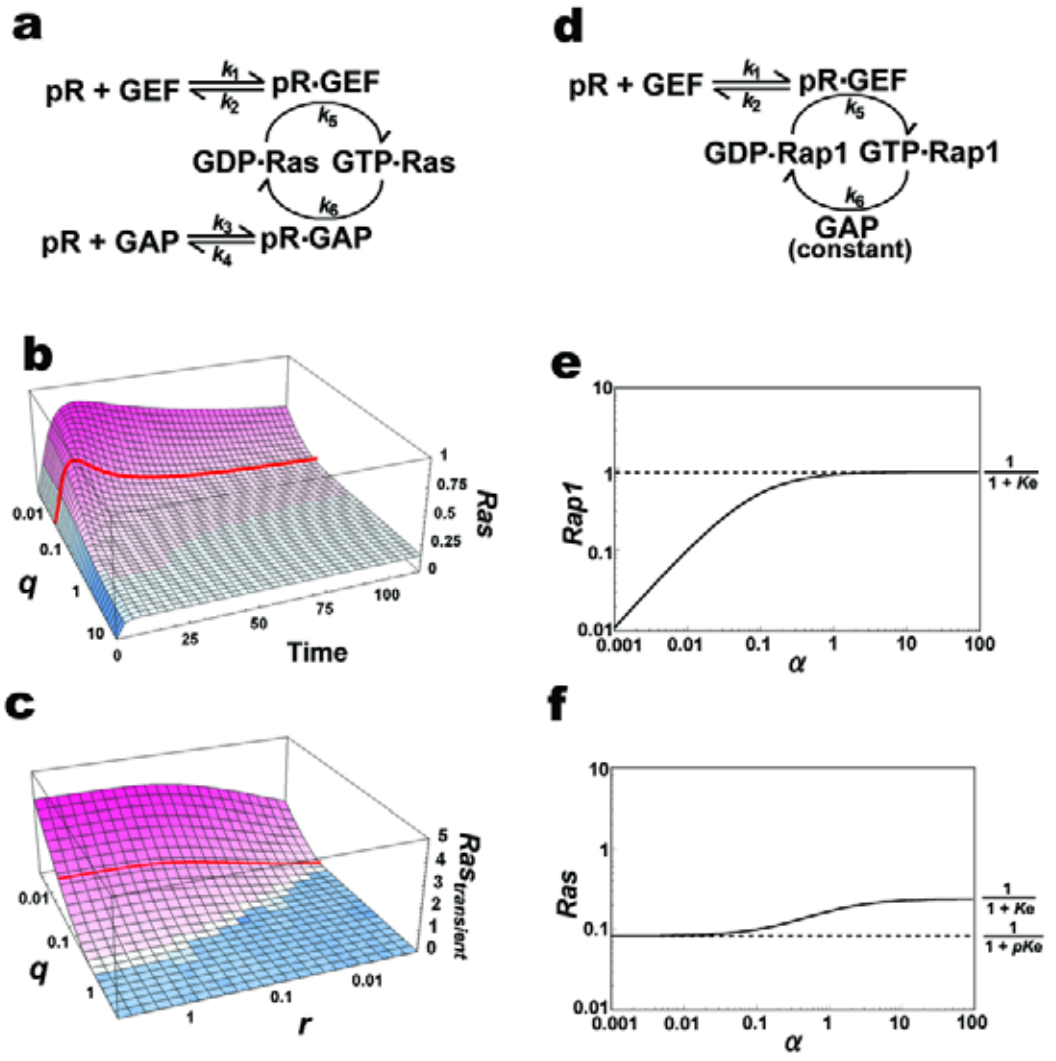

Figure 6 Characteristics of the Ras and Rap1 activation in the simple Ras and Rap1 models. (**a**) Simple Ras model, where pR-dependent GEF and GAP activation regulate Ras activation (Appendix A). (**b**) Constant *pR* stimulation was given, and *Ras* was plotted against the indicated values of *q*, where *q* indicates the inverse number of the relative time constant of the *GAP* activation compared to the *GEF* activation (Appendix B, Fig. S5). Here, Time denotes t/k_2. (**c**) $Ras_{transient}$ was plotted against the indicated values of *r* and *q*, where $Ras_{transient}$ and *r* indicate the relative peak amplitude of the transient *Ras* activation and the increasing rate of *pR*, respectively (Appendix B, Fig. S5). Red lines in **b** and **c** indicate the *Ras* activation with the equivalent parameters

in the *in silico* model (Appendix A). (**d**) Simple Rap1 model, where the pR-dependent GEF activation with constant GAP activity regulate Rap1 activation. (**e**) The *Rap1* activation at steady state derived from equation (1) where *pR* is given by a constant, α (Appendix A). (**f**) The *Ras* activation at steady state derived from equation (2) where *pR* is given by a constant, α (Appendix A).

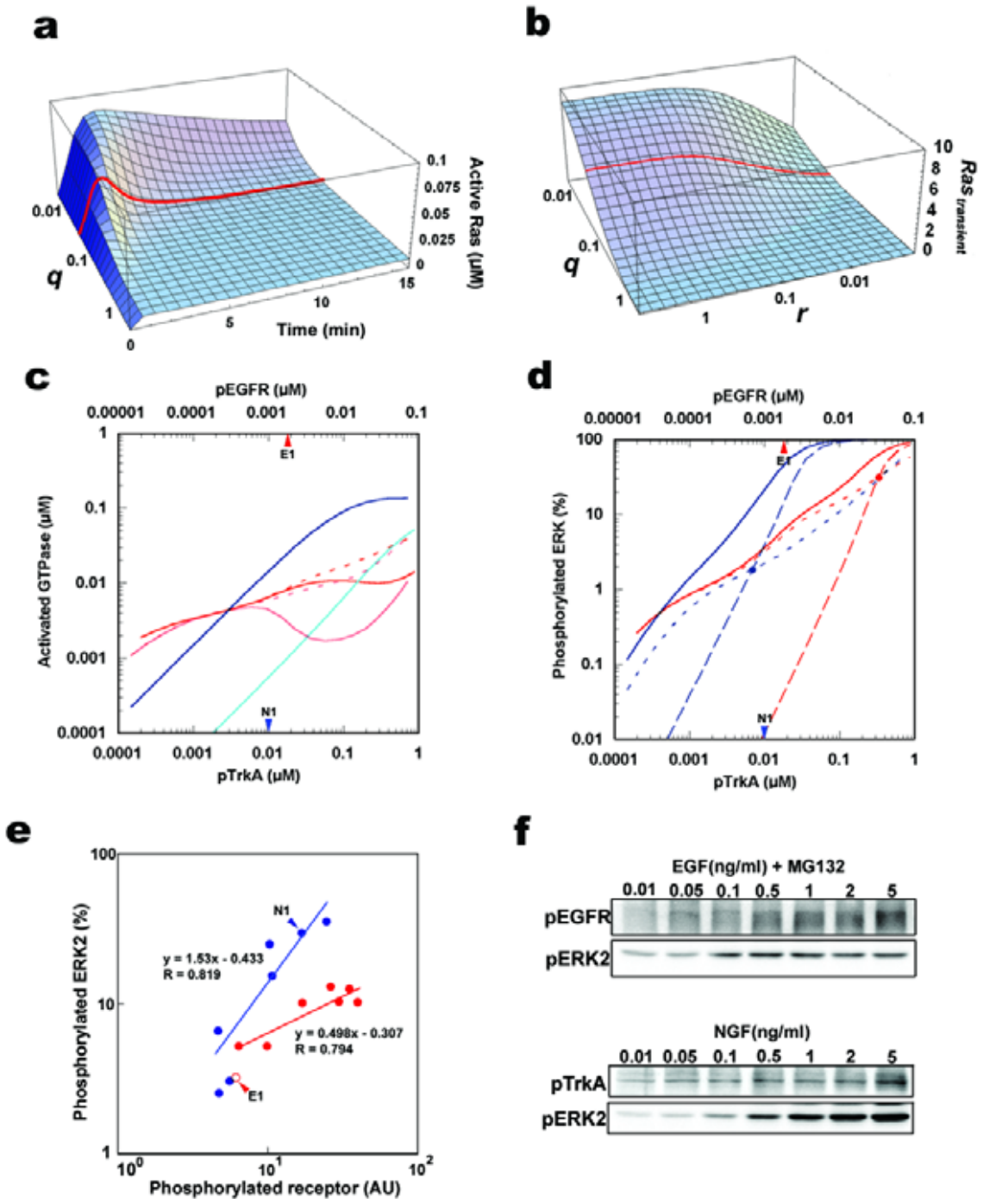

Figure 7 *In silico* dynamics of transient Ras activation and the Ras, Rap1, and ERK activations at steady state and the *in vivo* validation. (**a**) A constant phosphorylated EGFR stimulus was given, and the *in silico* Ras activation was plotted against the indicated values of *q*, where *q* indicates the inverse number of the relative time constant of the RasGAP activation (Appendix A). (**b**)

$Ras_{transient}$ was plotted against the indicated values of *r* and *q in silico*, where $Ras_{transient}$ and *r* indicate the relative peak amplitude of the transient Ras activation and the increasing rate of the phosphorylated EGFR, respectively (Appendix A). Red lines in **a** and **b** indicate the Ras activation with the original parameters in the *in silico* model. (**c**) Constant phosphorylated EGFR- and TrkA-dependent Ras and Rap1 activation at steady state *in silico*. The Ras and Rap1 activation against the phosphorylated EGFR are shown in red and cyan, and those against the phosphorylated TrkA are shown in pink and blue, respectively. Dashed lines indicate the Ras activation without negative feedback inhibition of SOS. (**d**) Constant phosphorylated EGFR- and TrkA-dependent ERK activation at steady state *in silico*. The ERK activation against the phosphorylated EGFR and TrkA are shown with red and blue solid lines, respectively. Dashed and dotted lines indicate the Rap1-dependent ERK activation (without Ras activation) and Ras-dependent ERK activation (without Rap1 activation), respectively. Circles indicate the intersecting points of the Ras- and Rap1-dependent ERK activation. (**e**) The *in vivo* ERK phosphorylation was plotted against the phosphorylated EGFR (red) and TrkA (blue) at 30 min. Lines were estimated by the least squares method. (**f**) The corresponding gels images of the results from **e**. Arrowheads in **c**-**e** indicate the points of the phosphorylated receptors induced by 1 ng/ml of EGF (in the absence of MG-132) and NGF, respectively.

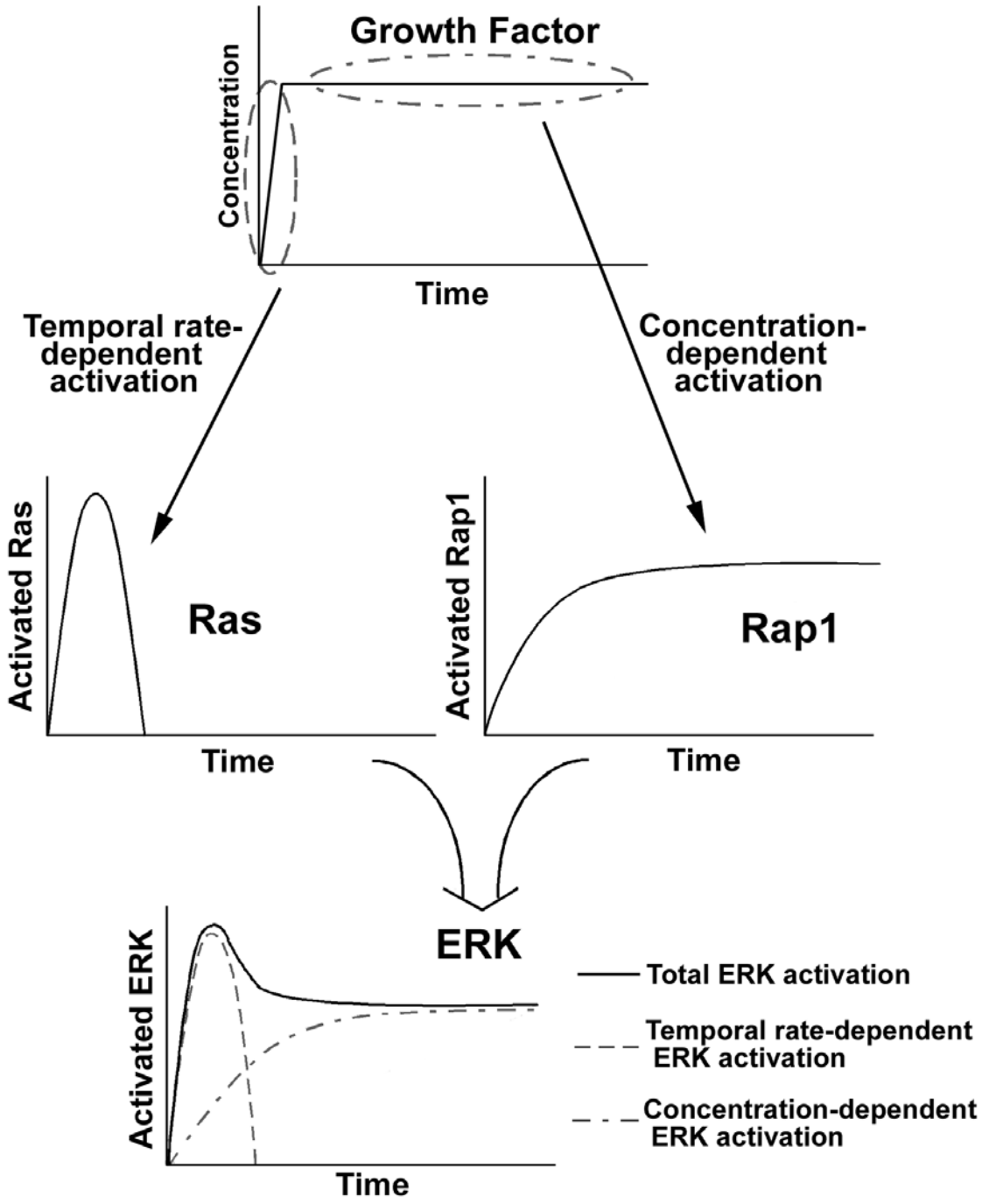

Figure 8 The distinct temporal dynamics of transient and sustained ERK activation via Ras and Rap1 activation. The Ras and Rap1 systems specifically capture the distinct properties of growth factors — the temporal rate and final concentration — and thereby encode these physical properties of growth factors into transient and sustained ERK activation, respectively.

Appendix A

In the simple Ras model in Figure 6a, the derivatives of pR·GEF and pR·GAP, and GTP·GTPase (Ras or Rap1) are given by

$$\frac{d[\mathrm{pR}\cdot\mathrm{GEF}]}{dt} = k_1[\mathrm{pR}]([\mathrm{GEF}_{\mathrm{total}}] - [\mathrm{pR}\cdot\mathrm{GEF}]) - k_2[\mathrm{pR}\cdot\mathrm{GEF}], \quad (3)$$

$$\frac{d[\mathrm{pR}\cdot\mathrm{GAP}]}{dt} = k_3[\mathrm{pR}]([\mathrm{GAP}_{\mathrm{total}}] - [\mathrm{pR}\cdot\mathrm{GAP}]) - k_4[\mathrm{pR}\cdot\mathrm{GAP}], \quad (4)$$

$$\frac{d[\mathrm{GTP}\cdot\mathrm{GTPase}]}{dt} = k_5[\mathrm{pR}\cdot\mathrm{GEF}]([\mathrm{GTPase}_{\mathrm{total}}] - [\mathrm{GTP}\cdot\mathrm{GTPase}]) - k_6[\mathrm{pR}\cdot\mathrm{GAP}][\mathrm{GTP}\cdot\mathrm{GTPase}], \quad (5)$$

where [ ] denotes the concentration of the molecule at time, *t*. The total concentration of GEF, GAP and GTPase ($[\mathrm{GEF}_{\mathrm{total}}]$, $[\mathrm{GAP}_{\mathrm{total}}]$ and $[\mathrm{GTPase}_{\mathrm{total}}]$, respectively) are conserved throughout the reactions. Equation (5) implicitly assumes that the concentration of GTPase complexed with either GEF or GAP is relatively small compared to the total concentration of the GTPases, GEF and GAP. Also, GEF and GAP implicitly represent pathways from the adaptor proteins to GEF or GAP, respectively. We write equations (3) – (5) in dimensionless form, with the following substitutions:

$$\frac{dGEF}{dt} = k_2\{pR - (1 + pR)GEF\}, \quad (3')$$

$$\frac{dGAP}{dt} = k_4\{p\cdot pR - (1 + p\cdot pR)GAP\}, \quad (4')$$

$$\frac{dGTPase}{dt} = k_6[\mathrm{GAP}_{\mathrm{total}}]\{GEF / \mathrm{Ke} - (GEF / \mathrm{Ke} + GAP)GTPase\}, \quad (5')$$

where pR=[pR]/Kd, GEF=[pR·GEF]/[GEF_{total}], GAP=[pR·GAP]/[GAP_{total}], $GTPase$ (Ras or $Rap1$)=[GTP·GTPase]/[$GTPase_{total}$], Kd=$k_2/k_1=pk_4/k_3$, Ke=$k_6[GAP_{total}]/k_5[GEF_{total}]$. Similarly, $s=k_6[GAP_{total}]/k_2$ represents the relative relaxation time constant of $GTPase$ compared to GEF where GEF and GAP are assumed to be constant. In addition, we define $q=k_4/k_2$ which represents the inverse number of the relative time constant of GAP activation compared to GEF activation because the inverse numbers of k_2 and k_4 represent the time constants of GEF and GAP activation (equations (3') and (4')), respectively, under the conditions where pR is a constant, ($pR=\alpha$), and GEF and GAP are not saturated ($\alpha<<1$, $p\alpha<<1$) (Fig. S5, see below). Unless specified, we set p=3.5, q=0.027, Ke=3.2, and s=2 in the simple Ras model (Fig. 6b, c, f) and Ke=0.09 in the simple Rap1 model (Fig. 6e), which are equivalent values in the *in silico* model (data not shown). We also set α=0.28 (Fig. 6b, c) which is equivalent to the concentration of phosphorylated EGFR induced by 1 ng/ml of EGF in the *in silico* model. The increasing pR stimulation is given by $pR=\alpha\{1-\exp(-rk_2t)\}$ where r corresponds to the increasing rate of pR (Fig. 6c, Fig. S5). The relative peak amplitude of the transient Ras activation, $Ras_{transient}$, is defined by $Ras_{transient}=(Max-Equi)/Equi$, where Max and $Equi$ denote Ras at the transient peak and steady state, respectively (Fig. 6c, Fig. 7b, Fig. S5). The transient Ras activation is defined by $Ras_{transient} > 0$ (Fig. 6c, Fig. 7b, Fig. S5). The increasing EGF stimuli led to the SOS and RasGAP activation in dose-dependent manner in EGF (Fig. 4a), indicating that the SOS and GAP activation were not saturated *in silico*. The equivalent conditions in the simple models can be obtained by $\alpha << 1$ and $p\alpha << 1$.

At steady state, the concentrations of the activated GEF, GAP and $GTPase$ become constant. Therefore, by setting the equations (3') - (5') equal to zero, we obtain equation

(2). Similarly, we obtain equation (1) from equations (3') and (5'), where *GAP* is always constant (*GAP*=1). Note that all values in Figure 6b, c, e and f are dimensionless.

In Figure 7a and b, we numerically measured the time constants of SOS and RasGAP activation, τ_{SOS} and τ_{RasGAP}, at which time constant EGF stimulation induced 50% of their maximal activation *in silico*, respectively. We defined $q = \tau_{SOS}/\ \tau_{RasGAP}$, which represents the inverse number of the relative time constant of the RasGAP activation compared to the SOS activation. Indicated values of q were obtained by changing τ_{RasGAP} without changing τ_{SOS}. The various values of τ_{RasGAP} were obtained by changing the *V*max of phosphorylation of Dok (Table S1a, 1), the time constants of the phosphorylated Dok-RasGAP interaction (Table S1c, 5) and of dephosphorylation of phosphorylated Dok (Table S1c, 6). For simplicity, the negative feedback inhibition of SOS by ERK was blocked for the analysis in Figure 7a and b, because the transient Ras activation was not dependent on the negative feedback (Fig. 5). We also set [phosphorylated EGFR]=0.0018 (μM), which corresponds to the phosphorylated EGFR concentration induced by 1 ng/ml of EGF for constant stimulation (Fig. 7a), and the increasing phosphorylated EGFR stimulus was given by

$[\text{phosphorylated EGFR}] = 0.0018\{1 - \exp(-r\frac{t}{\tau_{sos}})\}$ (μM) where r corresponds to the increasing rate of phosphorylated EGFR (Fig. 7b).

Appendix B

a

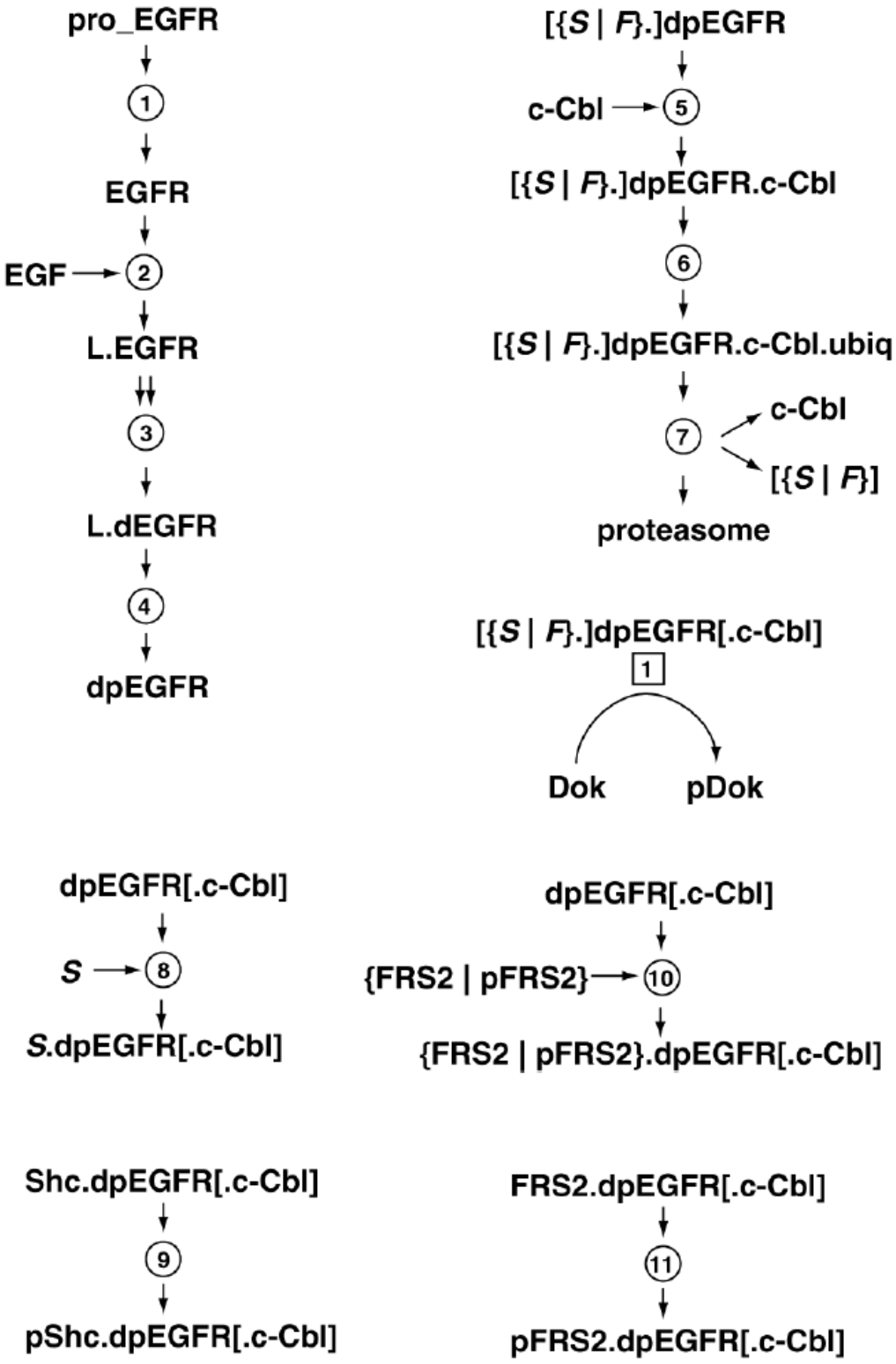

S and ***F*** denote **{Shc | [Grb2.SOS.]pShc}** and **{FRS2 | [Crk.C3G.]pFRS2}**, respectively.

b

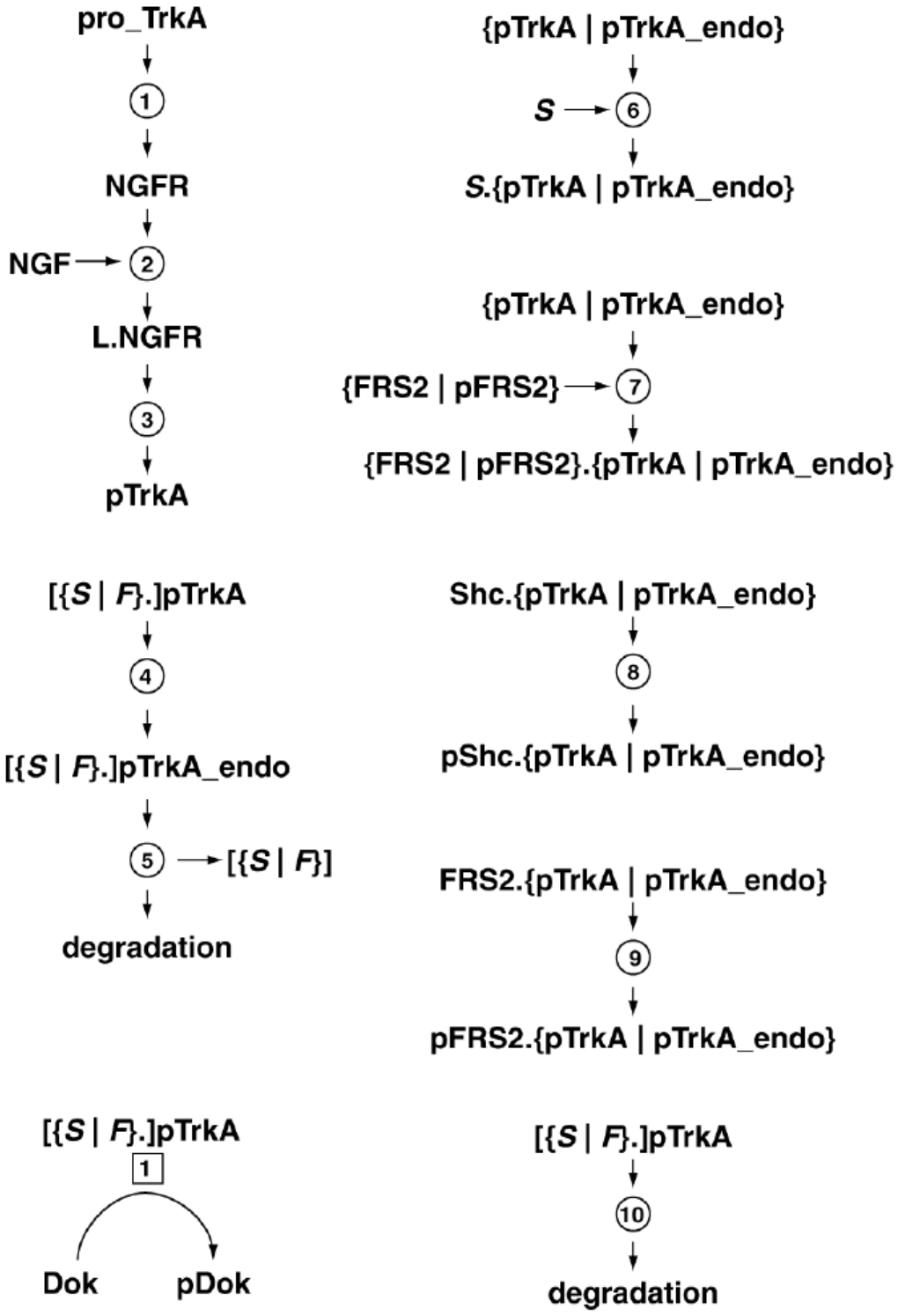

S and ***F*** denote **{Shc | [Grb2.SOS.]pShc}** and **{FRS2 | [Crk.C3G.]pFRS2}**, respectively.

c

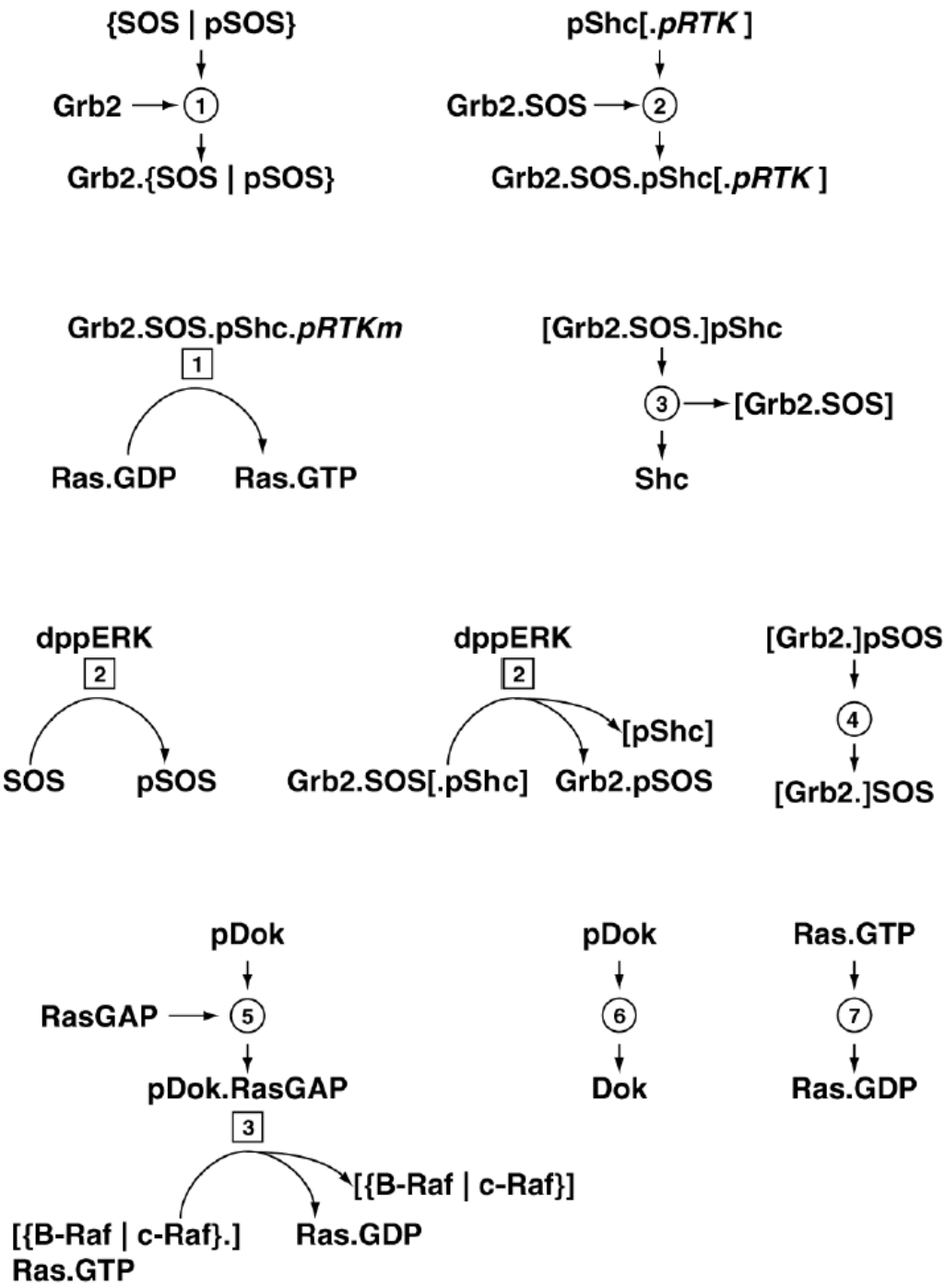

pRTKm and ***pRTK*** denote **{dpEGFR[.c-Cbl] | pTrkA}** and **{dpEGFR[.c-Cbl] | pTrkA | pTrkA_endo}**, respectively.

d

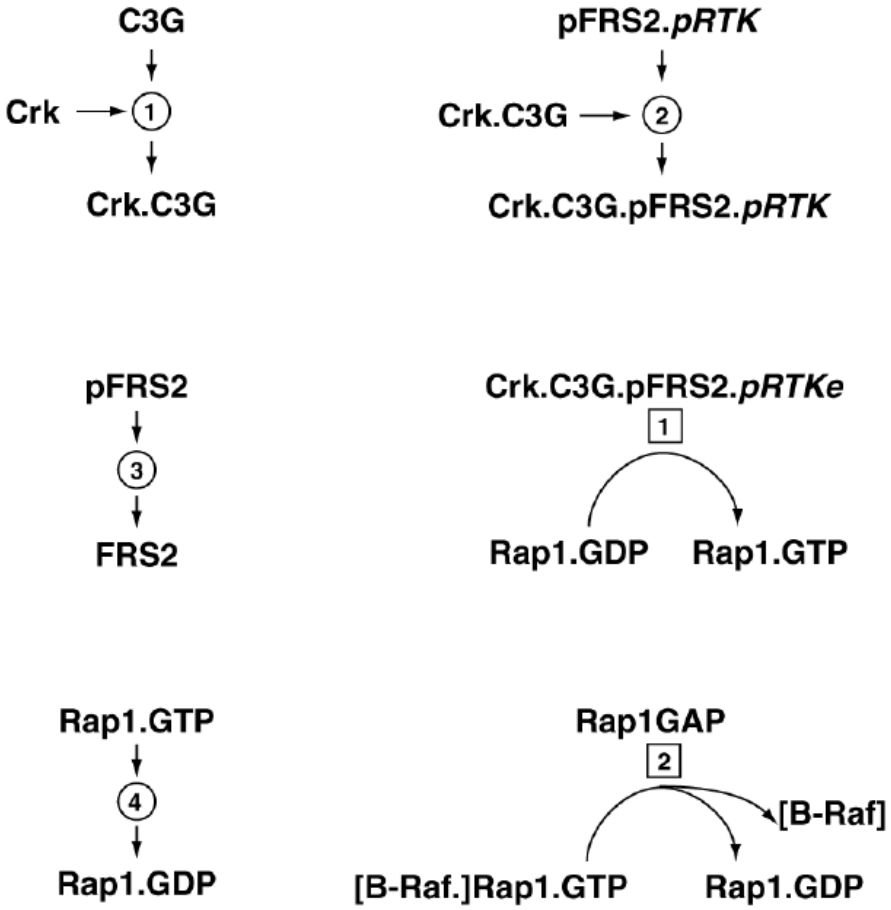

pRTKe and ***pRTK*** denote **{dpEGFR[.c-Cbl] | pTrkA_endo}** and **{dpEGFR[.c-Cbl] | pTrkA | pTrkA_endo}**, respectively.

e

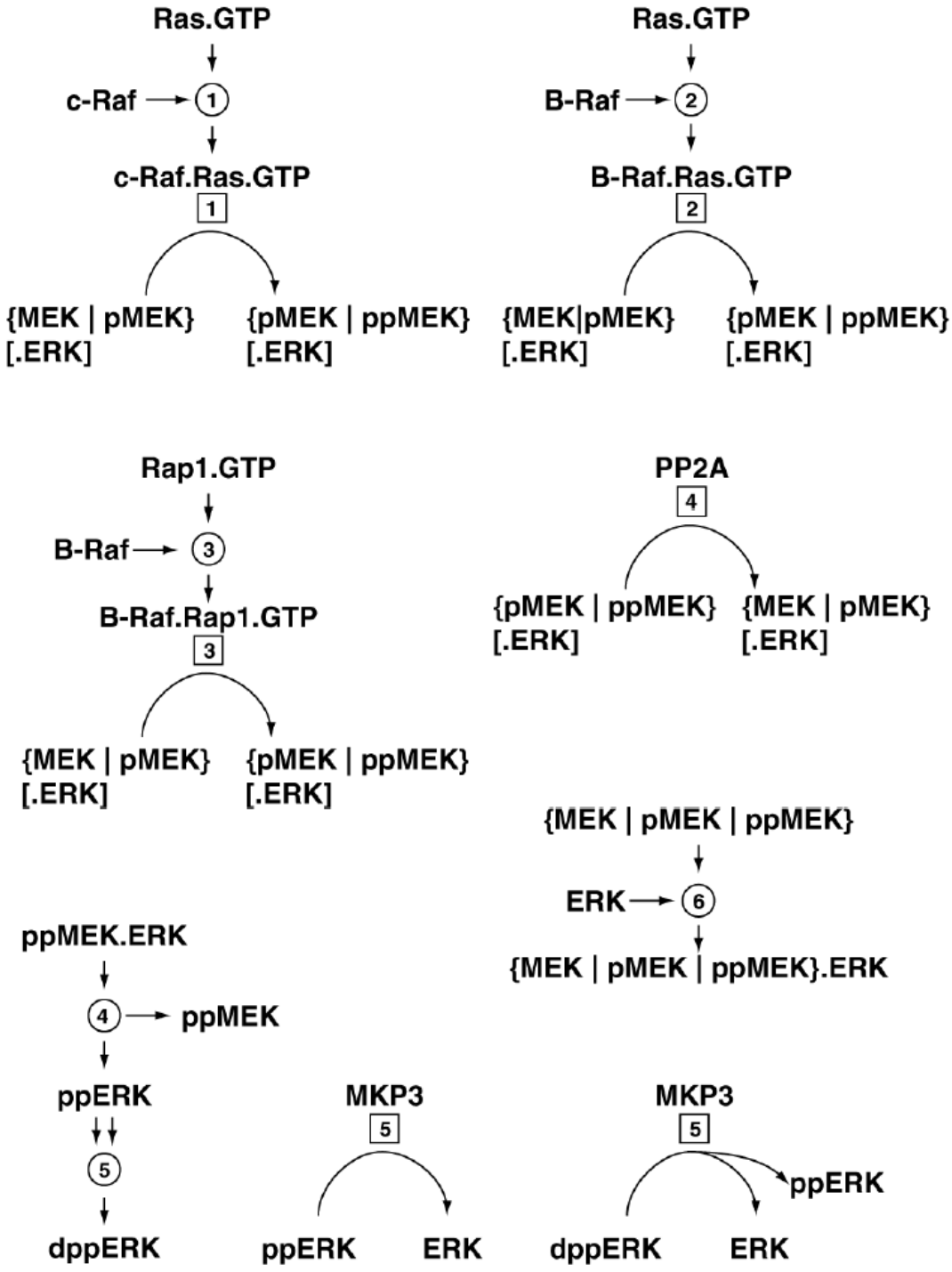
Ras.GTP
c-Raf
1
c-Raf.Ras.GTP
1
{MEK | pMEK}
[.ERK]
{pMEK | ppMEK}
[.ERK]
Ras.GTP
B-Raf
2
B-Raf.Ras.GTP
2
{MEK|pMEK}
[.ERK]
{pMEK | ppMEK}
[.ERK]
Rap1.GTP
B-Raf
3
B-Raf.Rap1.GTP
3
{MEK | pMEK}
[.ERK]
{pMEK | ppMEK}
[.ERK]
PP2A
4
{pMEK | ppMEK}
[.ERK]
{MEK | pMEK}
[.ERK]
{MEK | pMEK | ppMEK}
ERK
6
{MEK | pMEK | ppMEK}.ERK
ppMEK.ERK
4
ppMEK
ppERK
5
dppERK
MKP3
5
ppERK
ERK
MKP3
5
ppERK
dppERK
ERK

Notation of Figure S1

Circles with arrows denote molecule-molecule interactions. Boxes with round arrows denote enzymatic reactions. Rate constants (Numbered circles or boxes) and concentrations of molecules are shown in Appendix B, Table S1. Periods between molecules denote non-covalent binding. p and pp denote monophosphorylated and diphosphorylated molecules, respectively. d denotes a dimerised molecule. [ ] denotes an optional component(s) of the complex which shares the same kinetic parameters. For example, [pShc.[Sos.Grb2.]]pEGFR indicates either pEGFR alone, pShc.pEGFR, or pShc.Sos.Grb2.pEGFR. { | } denotes an exclusive component which shares the same kinetic parameters. For example, {SOS|pSOS} indicates either SOS or pSOS.

Figure S1a Tyrosine phosphorylation of EGFR and recruitment of adaptor proteins to EGFR. Binding of EGF to EGFR triggers the dimerisation of the receptors, resulting in autophosphorylation of the receptors[1]. Phosphorylated EGFR binds adaptor proteins including Shc[2], c-Cbl[3,4] and FRS2[5], and phosphorylates these adaptor proteins and Dok[6]. EGFR complexed with c-Cbl is ubiquitinated and degraded by proteasome[7-9]. *S* and *F* denote {Shc | [Grb2.Sos.]pShc} and {FRS2 | [Crk.C3G.]pFRS2}, respectively.

Figure S1b Tyrosine phosphorylation of TrkA and recruitment of adaptor proteins to TrkA. Binding of NGF to NGFR, consisting of TrkA and p75, triggers autophosphorylation of TrkA[10]. Phosphorylated TrkA binds adaptor proteins including Shc[11,12] and FRS2[13-15], and phosphorylates the adaptor proteins and Dok. Because the binding of Shc and FRS2 to TrkA compete[14,15], Shc and FRS2 exclusively bind TrkA in this model. Activated TrkA complexed with adaptor proteins is internalised to endosome where Rap1 is activated[16]. Internalisation of TrkA in this model is represented as a single exponetial decay, however, this implicitly represents the PI-3

kinase dependent internalisation of the TrkA[17]. *S* and *F* denote {Shc | [Grb2.Sos.]pShc} and {FRS2 | [Crk.C3G.]pFRS2}, respectively.

Figure S1c Activation of Ras. Grb2 and SOS complex[18-23] is recruited to phosphorylated Shc bound to EGFR[2] or TrkA[11,12] and catalyse GDP/GTP exchange reaction of Ras[18-23]. Activated ERK phosphorylates SOS[24,25] and phosphorylated SOS dissociates from the complex with Shc[26,27]. Sprouty[28,29] and Spred[30] have recently been shown to be involved in negative feedback inhibition of Ras. In this model, ERK-dependent negative feedback inhibition of SOS implicitly represents Sprouty-dependent negative feedback inhibition because these pathways can be computationally regarded as similar pathways. RasGAP recruited to phosphorylated Dok[6] facilitates intrinsic GTPase reaction of Ras[31]. Ras.GTP is also inactivated by intrinsic GTPase activity[31]. *pRTKm* and *pRTK* denote {dpEGFR[.c-Cbl] | pTrkA} and {dpEGFR[.c-Cbl] | pTrkA | pTrkA _endo}, respectively.

Figure S1d Activation of Rap1. Crk and C3G complex[32] is recruited to phosphorylated FRS2 bound to the receptors[14,33], and catalyse GDP/GTP exchange reaction of Rap1[34]. Rap1GAP facilitates intrinsic GTPase activity of Rap1[35]. Rap1.GTP is also inactivated by its intrinsic GTPase activity[31]. Recruitment of Crk and C3G complex to TrkA may involve other adaptor proteins including SHP[16,36], Gab2[16] and p130CAS[16,37]. In this model, FRS2-dependent recruitment of Crk and C3G complex to TrkA implicitly represents these similar pathways. *pRTKe* and *pRTK* denote {dpEGFR[.c-Cbl] | pTrkA_endo} and {dpEGFR[.c-Cbl] | pTrkA | pTrkA _endo}, respectively.

Figure S1e Activation of Raf, MEK and ERK. GTP-bound forms of Ras and Rap1 interact with c-Raf[38-43] and B-Raf[44-46], and B-Raf[47,48], respectively, and activated c-Raf

and B-Raf phosphorylate MEK. Phosphorylation of MEK at S218 and S222 (rat MEK1) results in activation of MEK[49-51]. Phosphorylated MEK is dephosphorylated by PP2A[52-55]. Unphosphorylated ERK forms complex with MEK[56,57]. Activated MEK phosphorylates ERK at T183 and Y185 (rat ERK2) and this dual phosphorylation leads to activation[58,59] release from the complex with MEK[60], and dimerisation[61] of ERK. Phosphorylated ERK is dephosphorylated by MKP3[62,63].

References

1. Schlessinger, J. Ligand-induced, receptor-mediated dimerization and activation of EGF receptor. *Cell* **110**, 669-672 (2002).
2. Rozakis-Adcock, M. *et al.* Association of the Shc and Grb2/Sem5 SH2-containing proteins is implicated in activation of the Ras pathway by tyrosine kinases. *Nature* **360**, 689-692 (1992).
3. Tanaka, S., Neff, L., Baron, R. & Levy, J. B. Tyrosine phosphorylation and translocation of the c-cbl protein after activation of tyrosine kinase signaling pathways. *J. Biol. Chem.* **270**, 14347-14351 (1995).
4. Galisteo, M. L., Dikic, I., Batzer, A. G., Langdon, W. Y. & Schlessinger, J. Tyrosine phosphorylation of the c-cbl proto-oncogene protein product and association with epidermal growth factor (EGF) receptor upon EGF stimulation. *J. Biol. Chem.* **270**, 20242-20245 (1995).
5. Wu, Y., Chen, Z. & Ullrich, A. EGFR and FGFR signaling through FRS2 is subject to negative feedback control by ERK1/2. *Biol. Chem.* **384**, 1215-1226 (2003).
6. Jones, N. & Dumont, D. J. Recruitment of Dok-R to the EGF receptor through its PTB domain is required for attenuation of Erk MAP kinase activation. *Curr. Biol.* **9**, 1057-1060 (1999).
7. Levkowitz, G. *et al.* c-Cbl/Sli-1 regulates endocytic sorting and ubiquitination of the epidermal growth factor receptor. *Genes Dev.* **12**, 3663-3674 (1998).
8. Waterman, H. & Yarden, Y. Molecular mechanisms underlying endocytosis and sorting of ErbB receptor tyrosine kinases. *FEBS Lett.* **490**, 142-152 (2001).
9. Di Fiore, P. P. & Gill, G. N. Endocytosis and mitogenic signaling. *Curr. Opin. Cell. Biol.* **11**, 483-488 (1999).
10. Kaplan, D. R. & Miller, F. D. Signal transduction by the neurotrophin receptors. *Curr. Opin. Cell Biol.* **9**, 213-221 (1997).
11. Obermeier, A. *et al.* Neuronal differentiation signals are controlled by nerve growth factor receptor/Trk binding sites for SHC and PLC gamma. *EMBO J.* **13**, 1585-1590 (1994).
12. Stephens, R. M. *et al.* Trk receptors use redundant signal transduction pathways involving SHC and PLC-gamma 1 to mediate NGF responses. *Neuron* **12**, 691-705 (1994).

13. Kouhara, H. *et al.* A lipid-anchored Grb2-binding protein that links FGF-receptor activation to the Ras/MAPK signaling pathway. *Cell* **89**, 693-702 (1997).
14. Meakin, S. O., MacDonald, J. I., Gryz, E. A., Kubu, C. J. & Verdi, J. M. The signaling adapter FRS-2 competes with Shc for binding to the nerve growth factor receptor TrkA. A model for discriminating proliferation and differentiation. *J. Biol. Chem.* **274**, 9861-9870 (1999).
15. Ong, S. H. *et al.* FRS2 proteins recruit intracellular signaling pathways by binding to diverse targets on fibroblast growth factor and nerve growth factor receptors. *Mol. Cell. Biol.* **20**, 979-989 (2000).
16. Wu, C., Lai, C. F. & Mobley, W. C. Nerve growth factor activates persistent Rap1 signaling in endosomes. *J. Neurosci.* **21**, 5406-54016 (2001).
17. York, R. D. *et al.* Role of phosphoinositide 3-kinase and endocytosis in nerve growth factor-induced extracellular signal-regulated kinase activation via Ras and Rap1. *Mol. Cell. Biol.* **20**, 8069-8083 (2000).
18. Egan, S. E. *et al.* Association of Sos Ras exchange protein with Grb2 is implicated in tyrosine kinase signal transduction and transformation. *Nature* **363**, 45-51 (1993).
19. Rozakis-Adcock, M., Fernley, R., Wade, J., Pawson, T. & Bowtell, D. The SH2 and SH3 domains of mammalian Grb2 couple the EGF receptor to the Ras activator mSos1. *Nature* **363**, 83-85 (1993).
20. Li, N. *et al.* Guanine-nucleotide-releasing factor hSos1 binds to Grb2 and links receptor tyrosine kinases to Ras signalling. *Nature* **363**, 85-88 (1993).
21. Gale, N. W., Kaplan, S., Lowenstein, E. J., Schlessinger, J. & Bar-Sagi, D. Grb2 mediates the EGF-dependent activation of guanine nucleotide exchange on Ras. *Nature* **363**, 88-92 (1993).
22. Buday, L. & Downward, J. Epidermal growth factor regulates p21ras through the formation of a complex of receptor, Grb2 adapter protein, and Sos nucleotide exchange factor. *Cell* **73**, 611-20 (1993).
23. Chardin, P. *et al.* Human Sos1: a guanine nucleotide exchange factor for Ras that binds to GRB2. *Science* **260**, 1338-1343 (1993).
24. Langlois, W. J., Sasaoka, T., Saltiel, A. R. & Olefsky, J. M. Negative feedback regulation and desensitization of insulin- and epidermal growth factor-stimulated p21ras activation. *J. Biol. Chem.* **270**, 25320-25323 (1995).
25. Waters, S. B. *et al.* Desensitization of Ras activation by a feedback disassociation of the SOS-Grb2 complex. *J. Biol. Chem.* **270**, 20883-20886 (1995).
26. Holt, K. H. *et al.* Epidermal growth factor receptor targeting prevents uncoupling of the Grb2-SOS complex. *J. Biol. Chem.* **271**, 8300-8306 (1996).
27. Waters, S. B. *et al.* Insulin and epidermal growth factor receptors regulate distinct pools of Grb2-SOS in the control of Ras activation. *J. Biol. Chem.* **271**, 18224-18230 (1996).
28. Gross, I., Bassit, B., Benezra, M. & Licht, J. D. Mammalian sprouty proteins inhibit cell growth and differentiation by preventing ras activation. *J. Biol. Chem.* **276**, 46460-46468 (2001).
29. Hanafusa, H., Torii, S., Yasunaga, T. & Nishida, E. Sprouty1 and Sprouty2 provide a control mechanism for the Ras/MAPK signalling pathway. *Nat. Cell Biol.* **4**, 850-858 (2002).

30. Wakioka, T. *et al.* Spred is a Sprouty-related suppressor of Ras signalling. *Nature* **412**, 647-651 (2001).
31. Bourne, H. R., Sanders, D. A. & McCormick, F. The GTPase superfamily: conserved structure and molecular mechanism. *Nature* **349**, 117-127 (1991).
32. Tanaka, S. *et al.* C3G, a guanine nucleotide-releasing protein expressed ubiquitously, binds to the Src homology 3 domains of CRK and GRB2/ASH proteins. *Proc. Natl. Acad. Sci. U.S.A.* **91**, 3443-3447 (1994).
33. Kao, S., Jaiswal, R. K., Kolch, W. & Landreth, G. E. Identification of the mechanisms regulating the differential activation of the mapk cascade by epidermal growth factor and nerve growth factor in PC12 cells. *J. Biol. Chem.* **276**, 18169-18177 (2001).
34. Matsuda, M. *et al.* CRK protein binds to two guanine nucleotide-releasing proteins for the Ras family and modulates nerve growth factor-induced activation of Ras in PC12 cells. *Mol. Cell. Biol.* **14**, 5495-5500 (1994).
35. Rubinfeld, B. *et al.* Molecular cloning of a GTPase activating protein specific for the Krev-1 protein p21rap1. *Cell* **65**, 1033-1042 (1991).
36. Hadari, Y. R., Kouhara, H., Lax, I. & Schlessinger, J. Binding of Shp2 tyrosine phosphatase to FRS2 is essential for fibroblast growth factor-induced PC12 cell differentiation. *Mol. Cell. Biol.* **18**, 3966-3973 (1998).
37. Sakai, R. *et al.* A novel signaling molecule, p130, forms stable complexes in vivo with v-Crk and v-Src in a tyrosine phosphorylation-dependent manner. *EMBO J.* **13**, 3748-3756 (1994).
38. Moodie, S. A., Willumsen, B. M., Weber, M. J. & Wolfman, A. Complexes of Ras.GTP with Raf-1 and mitogen-activated protein kinase kinase. *Science* **260**, 1658-1661 (1993).
39. Zhang, X. F. *et al.* Normal and oncogenic p21ras proteins bind to the amino-terminal regulatory domain of c-Raf-1. *Nature* **364**, 308-313 (1993).
40. Warne, P. H., Viciana, P. R. & Downward, J. Direct interaction of Ras and the amino-terminal region of Raf-1 in vitro. *Nature* **364**, 352-355 (1993).
41. Van Aelst, L., Barr, M., Marcus, S., Polverino, A. & Wigler, M. Complex formation between RAS and RAF and other protein kinases. *Proc. Natl. Acad. Sci. U.S.A.* **90**, 6213-6217 (1993).
42. Vojtek, A. B., Hollenberg, S. M. & Cooper, J. A. Mammalian Ras interacts directly with the serine/threonine kinase Raf. *Cell* **74**, 205-214 (1993).
43. Koide, H., Satoh, T., Nakafuku, M. & Kaziro, Y. GTP-dependent association of Raf-1 with Ha-Ras: identification of Raf as a target downstream of Ras in mammalian cells. *Proc. Natl. Acad. Sci. U.S.A.* **90**, 8683-8686 (1993).
44. Jaiswal, R. K., Moodie, S. A., Wolfman, A. & Landreth, G. E. The mitogen-activated protein kinase cascade is activated by B-Raf in response to nerve growth factor through interaction with p21ras. *Mol. Cell. Biol.* **14**, 6944-6953 (1994).
45. Moodie, S. A., Paris, M. J., Kolch, W. & Wolfman, A. Association of MEK1 with p21ras.GMPPNP is dependent on B-Raf. *Mol. Cell. Biol.* **14**, 7153-7162 (1994).
46. Yamamori, B. *et al.* Purification of a Ras-dependent mitogen-activated protein kinase kinase kinase from bovine brain cytosol and its identification as a complex of B-Raf and 14-3-3 proteins. *J. Biol. Chem.* **270**, 11723-11726 (1995).

47. Ohtsuka, T., Shimizu, K., Yamamori, B., Kuroda, S. & Takai, Y. Activation of brain B-Raf protein kinase by Rap1B small GTP-binding protein. *J. Biol. Chem.* **271**, 1258-1261 (1996).
48. Vossler, M. R. *et al.* cAMP activates MAP kinase and Elk-1 through a B-Raf- and Rap1-dependent pathway. *Cell* **89**, 73-82 (1997).
49. Alessi, D. R. *et al.* Identification of the sites in MAP kinase kinase-1 phosphorylated by p74raf-1. *EMBO J.* **13**, 1610-1619 (1994).
50. Cowley, S., Paterson, H., Kemp, P. & Marshall, C. J. Activation of MAP kinase kinase is necessary and sufficient for PC12 differentiation and for transformation of NIH 3T3 cells. *Cell* **77**, 841-852 (1994).
51. Zheng, C. F. & Guan, K. L. Activation of MEK family kinases requires phosphorylation of two conserved Ser/Thr residues. *EMBO J.* **13**, 1123-1131 (1994).
52. Gomez, N. & Cohen, P. Dissection of the protein kinase cascade by which nerve growth factor activates MAP kinases. *Nature* **353**, 170-173 (1991).
53. Shirakabe, K., Gotoh, Y. & Nishida, E. A mitogen-activated protein (MAP) kinase activating factor in mammalian mitogen-stimulated cells is homologous to Xenopus M phase MAP kinase activator. *J. Biol. Chem.* **267**, 16685-16690 (1992).
54. Seger, R. *et al.* Purification and characterization of mitogen-activated protein kinase activator(s) from epidermal growth factor-stimulated A431 cells. *J. Biol. Chem.* **267**, 14373-14381 (1992).
55. Crews, C. M. & Erikson, R. L. Purification of a murine protein-tyrosine/threonine kinase that phosphorylates and activates the Erk-1 gene product: relationship to the fission yeast byr1 gene product. *Proc. Natl. Acad. Sci. U.S.A.* **89**, 8205-8209 (1992).
56. Fukuda, M., Gotoh, Y. & Nishida, E. Interaction of MAP kinase with MAP kinase kinase: its possible role in the control of nucleocytoplasmic transport of MAP kinase. *EMBO J.* **16**, 1901-1908 (1997).
57. Rubinfeld, H., Hanoch, T. & Seger, R. Identification of a cytoplasmic-retention sequence in ERK2. *J. Biol. Chem.* **274**, 30349-30352 (1999).
58. Davis, R. J. The mitogen-activated protein kinase signal transduction pathway. *J. Biol. Chem.* **268**, 14553-14556 (1993).
59. Nishida, E. & Gotoh, Y. The MAP kinase cascade is essential for diverse signal transduction pathways. *Trends Biochem. Sci.* **18**, 128-131 (1993).
60. Adachi, M., Fukuda, M. & Nishida, E. Two co-existing mechanisms for nuclear import of MAP kinase: passive diffusion of a monomer and active transport of a dimer. *EMBO J.* **18**, 5347-5358 (1999).
61. Khokhlatchev, A. V. *et al.* Phosphorylation of the MAP kinase ERK2 promotes its homodimerization and nuclear translocation. *Cell* **93**, 605-615 (1998).
62. Zhao, Y. & Zhang, Z. Y. The mechanism of dephosphorylation of extracellular signal-regulated kinase 2 by mitogen-activated protein kinase phosphatase 3. *J. Biol. Chem.* **276**, 32382-32391 (2001).
63. Farooq, A. & Zhou, M. M. Structure and regulation of MAPK phosphatases. *Cell. Signal.* **16**, 769-779 (2004).

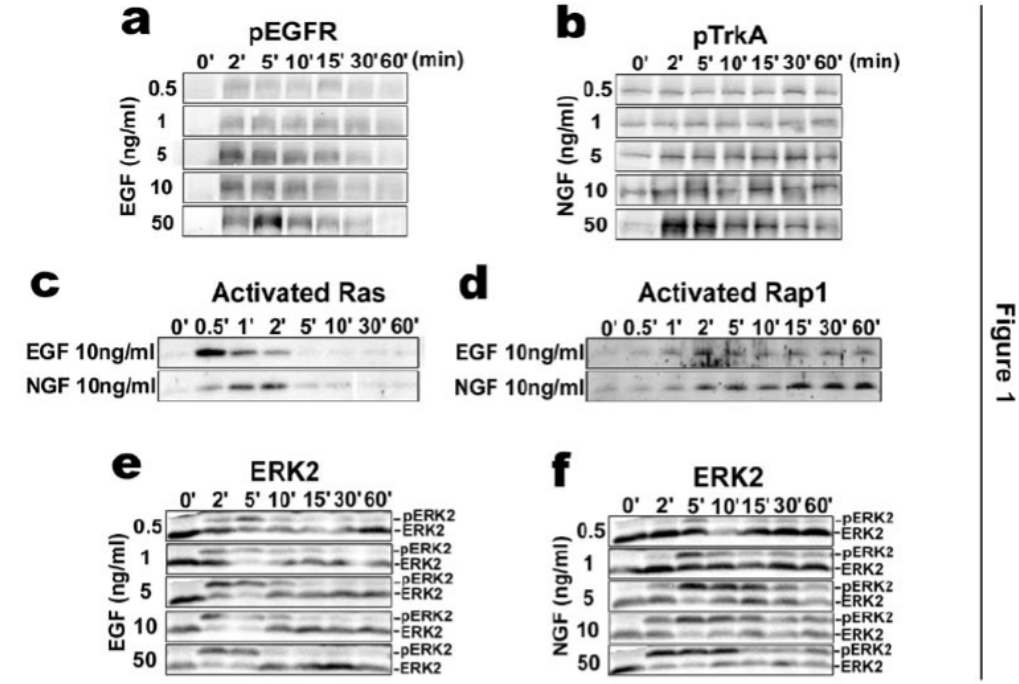

Figure 1

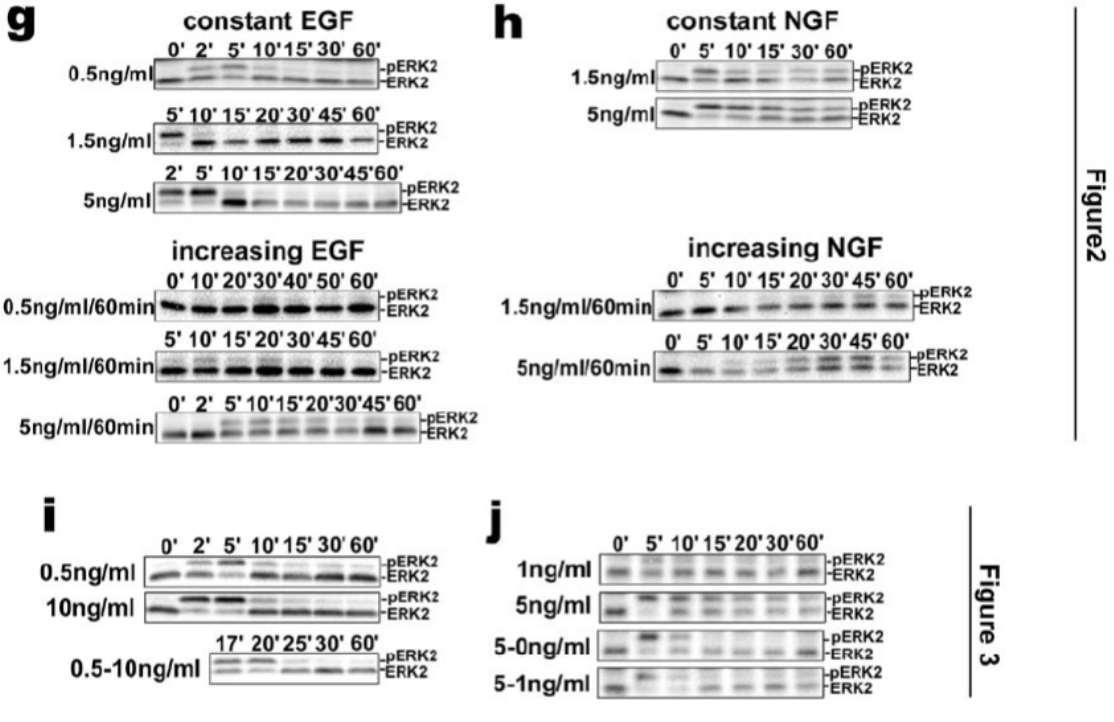

Figure2

Figure 3

Figure 4

Figure S2 Images of the original gels in Fig. 1, Fig. 2, Fig. 3 and Fig. 4. (**a**) phosphorylated EGFR at Y1068 (pEGFR) (Fig. 1b), (**b**) phosphorylated TrkA at Y490 (pTrkA) (Fig. 1c), (**c**) activated Ras (Fig. 1f), (**d**) activated Rap1 (Fig. 1g), (**e**) EGF-induced phosphorylated and nonphosphorylated ERK2 (pERK2 and ERK2) (Fig. 1h), (**f**) NGF-induced phosphorylated and nonphosphorylated ERK2 (Fig. 1i), (**g**) constant and increasing EGF stimuli-induced ERK2 activation (Fig. 2a), (**h**) constant and increasing NGF stimuli-induced ERK2 activation (Fig. 2b), (**i**) a stepwise increase of EGF stimuli-induced ERK2 activation (Fig. 3a), (**j**) a stepwise decrease of NGF stimuli-induced ERK2 activation (Fig. 3b), and (**k**) constant EGF stimuli-induced SOS and Ras GAP recruitment to the membrane fractions (Fig. 4c). Since the temporal patterns of phosphorylated ERK1 and ERK2 were always similar (data not shown), phosphorylated ERK2 per total ERK2 were plotted for all figures.

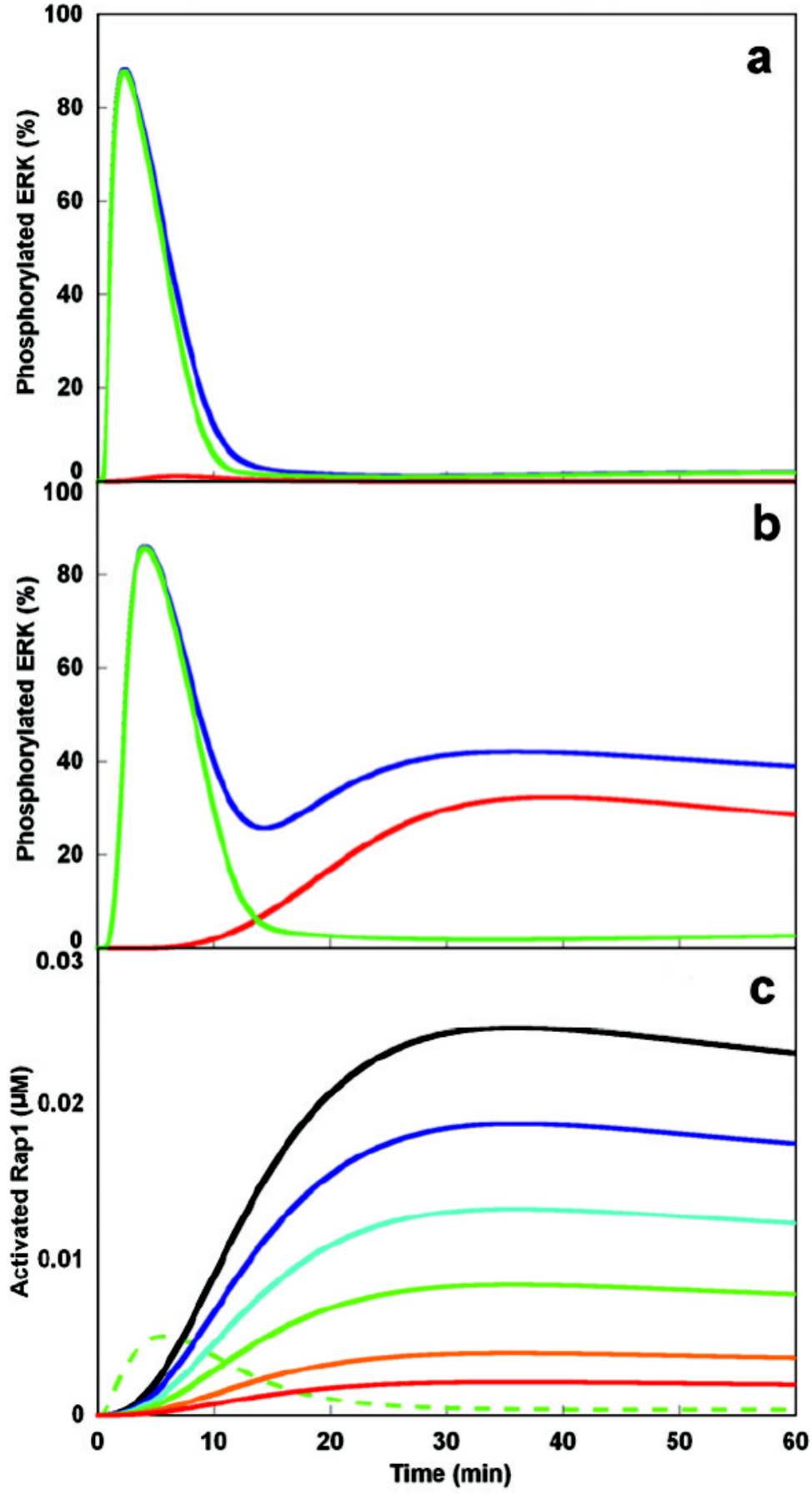
a
b
c
Phosphorylated ERK (%)
Phosphorylated ERK (%)
Activated Rap1 (μM)
Time (min)
0
20
40
60
80
100
0
0.01
0.02
0.03
0
10
20
30
40
50
60

Figure S3 The roles of Ras and Rap1 in EGF- and NGF-dependent ERK activation *in silico*. Concentration of the activated Ras or Rap1 was fixed at the basal level, and then simulations were run with (**a**) EGF (10 ng/ml) and (**b**) NGF (10 ng/ml), and phosphorylation of ERK was plotted. Blue line, normal conditions; green line, without Rap1 activation; red line, without Ras activation. (**c**) Rap1 activation depends on the affinity of FRS2 for the phosphorylated receptors. The dissociation constant of FRS2 for phosphorylated TrkA was set at 20, 50, 100, 200, 500 or 1000 nM. Then, the constant NGF stimulus (10 ng/ml) was given and the activation of Rap1 was plotted. The black, blue, cyan, green, orange and red lines indicate the Rap1 activation with 20, 50, 100, 200, 500 or 1000 nM of the dissociation constant of FRS2 for phosphorylated TrkA, respectively. Green dashed line indicates the Rap1 activation in response to EGF (10ng/ml) *in silico* where the affinity of FRS2 for phosphorylated EGFR was 200 nM (Fig. 1g). Note that 20 and 200 nM were the original dissociation constants of FRS2 for phosphorylated TrkA and EGFR *in silico*, respectively (Table S1).

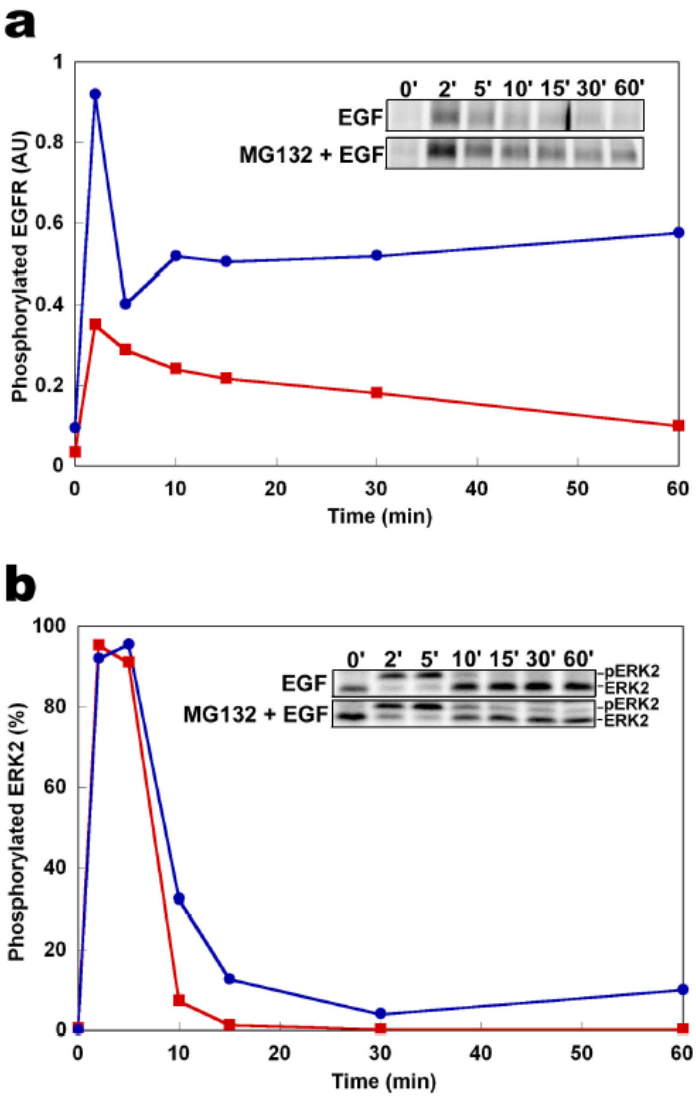
a
Phosphorylated EGFR (AU)
Time (min)
0' 2' 5' 10' 15' 30' 60'
EGF
MG132 + EGF
b
Phosphorylated ERK2 (%)
Time (min)
0' 2' 5' 10' 15' 30' 60'
EGF
MG132 + EGF
pERK2
ERK2
pERK2
ERK2
c
0 min
EGF 30sec
EGF 30min
MG132 + EGF 30min
GTP-Ras
(fold) 1.0 14.8 2.3 6.3
d
0 min
EGF 30min
MG132 + EGF 30min
NGF 30min
GTP-Rap1
(fold) 1.0 1.8 2.8 3.9

Figure S4 Sustained Ras, Rap1 and ERK activation in response to the sustained phosphorylated EGFR. (**a, b**) Fifty μM of MG-132, a proteasome inhibitor, was added for 1h, then PC12 cells were stimulated with EGF (10ng/ml). After stimulation, phosphorylated EGFR (**a**) and phosphorylated ERK2 (**b**) were measured. Blue and red lines indicate the responses in the presence or absence of MG-132, respectively. MG-132 alone did not affect the amounts of total and phosphorylated EGFR during incubation for 120 min (data not shown). Sustained Ras (**c**) and Rap1 (**d**) activation in the presence of MG-132 at 30 min after stimulation under the same conditions in (a).

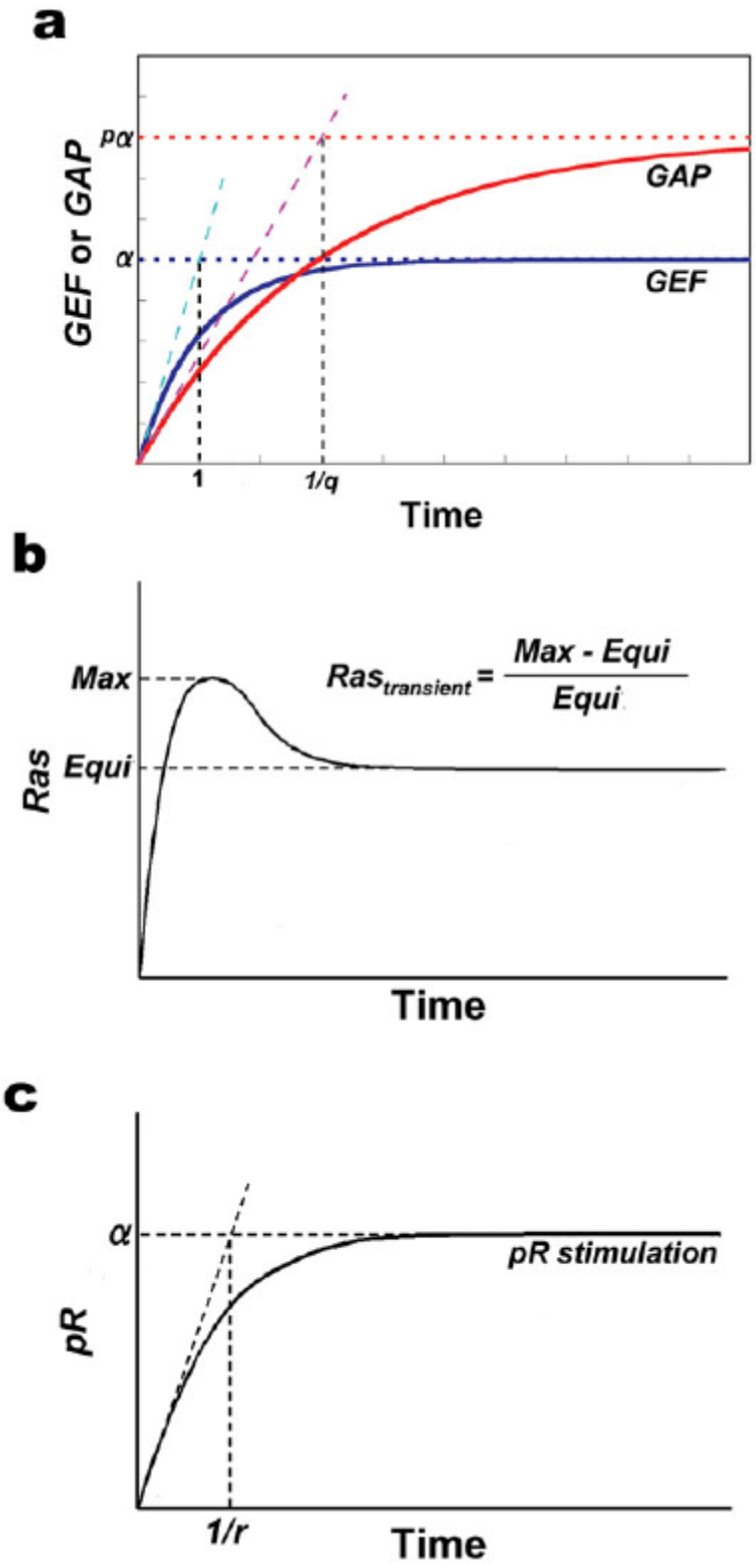
a
pα
α
GEF or GAP
GAP
GEF
1
1/q
Time
b
Max
Equi
Ras
Ras transient = Max - Equi / Equi
Time
c
α
pR
pR stimulation
1/r
Time

Figure S5 Transient *Ras* activation in the simple Ras model. (**a**) Schematic representation of the *GEF* activation and *GAP* activation in response to the constant *pR* stimulation. The relative dimensionless time constants of *GEF* and *GAP* are 1 and 1/*q*, respectively, under the conditions where $\alpha << 1$ and $p\alpha << 1$ (Appendix A). Thus, *q* can be regarded as the inverse number of the relative time constant of *GAP* compared to *GEF*. The dimensionless concentrations of *GEF* and *GAP* at steady state are given by α and $p\alpha$, respectively. Red and blue lines indicate *GAP* and *GEF*, respectively. (**b**) The definition of the characteristics of the transient *Ras* activation. The relative amplitude of the transient *Ras* activation compared to that at steady state was defined by $Ras_{transinet}$, which is given by $Ras_{transinet}=(Max-Equi)/Equi$ (Appendix A). Here, the transient *Ras* activation was defined by $Ras_{transinet} >0$. (**c**) Increasing *pR* stimulation used in Figure 6b and c. The *pR* stimulation was given by $pR= \alpha\{1-\exp(-rk_2t)\}$ (Appendix A). Note that *r* corresponds to the increasing rate of *pR*. Time in **a**-**c** denotes t/k_2.

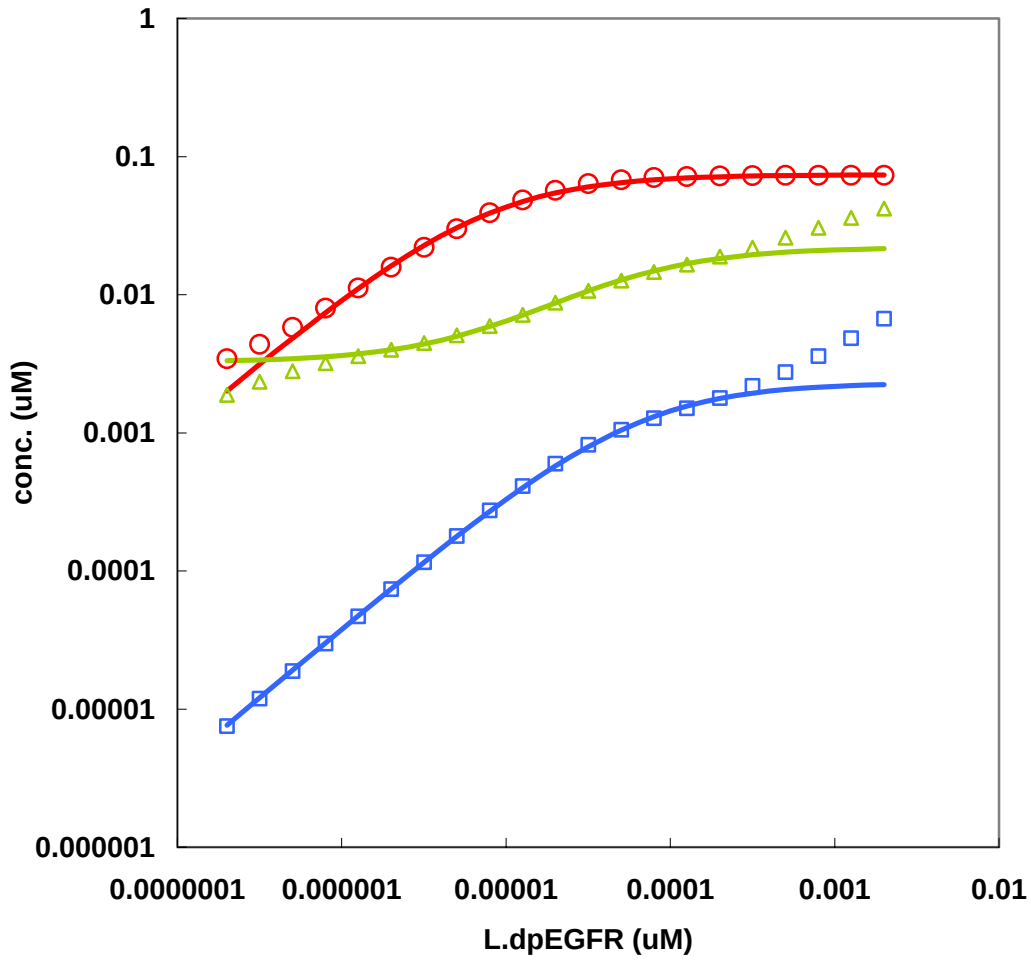

Figure S6 Dose-dependent activation of molecules *in silico* and in the simple Ras model at steady state. Blue boxes, red circles and green triangles indicate SOS, RasGAP and Ras activation against indicated phosphorylated EGFR at steady state *in silico*. Solid blue, red and green lines indicate pR·GEF, pR·GAP and GTP·Ras activation in the simple Ras model where equivalent parameters were given (Appendix A).

Table S1a

Molecule-molecule interaction	Reaction number	kf (/s/μM)	kb (/s)	Notes
	1	1.0e-4 *	1.0e-4	Constrained by *in vivo* dynamics of EGFR (Fig. 1b)
	2	2.2833	0.0029666	[1,2]
	3	10	0.02	[3,4]
	4	4	0.001	[3,5,6]
	5	0.5	0.2	On the basis of[7], further constrained by *in vivo* dynamics of EGFR (Fig. 1b)
	6	0.05 *		On the basis of[7], further constrained by *in vivo* dynamics of EGFR (Fig. 1b)
	7	0.001 *		Constrained by *in vivo* dynamics of EGFR (Fig. 1b)
	8	10	0.2	[3,4]
	9	1 *		On the basis of[8], further constrained by *in vivo* dynamics of Ras (Fig. 1f)
	10	1	0.2	On the basis of[9], further constrained by EGF-dependent Rap1 activation (Fig. 1g)
	11	1 *		On the basis of[9], further constrained by EGF-dependent Rap1 activation (Fig. 1g)
	* denotes /s.			

Enzymatic reaction	Reaction number	Km (μM)	Vmax (/s)	Notes
	1	0.1	0.2	[10]

Initial concentration	Molecule	CoInit (μM)		Notes
	EGFR	0.3		[3]
	pro_EGFR	0.3	constant	[3,11]
	Shc	1		[3]
	c-Cbl	0.5		On the basis of[12], futher constrained by *in vivo* dynamics of EGFR (Fig. 1b)
	FRS2	1		[13]
	Dok	0.3		Constrained by *in vivo* dynamics of Ras (Fig. 1f)

1 French, A. R., Tadaki, D. K., Niyogi, S. K. & Lauffenburger, D. A. Intracellular trafficking of epidermal growth factor family ligands is directly influenced by the pH sensitivity of the receptor/ligand interaction. *J. Biol. Chem.* **270**, 4334-4340 (1995).

2 DeWitt, A. et al. Affinity regulates spatial range of EGF receptor autocrine ligand binding. *Dev. Biol.* **250**, 305-316 (2002).

3 Bhalla, U. S. & Iyengar, R. Emergent properties of networks of biological signaling pathways. *Science* **283**, 381-387 (1999).

4 Sasaoka, T., Langlois, W. J., Leitner, J. W., Draznin, B. & Olefsky, J. M. The signaling pathway coupling epidermal growth factor receptors to activation of p21ras. *J. Biol. Chem.* **269**, 32621-32625 (1994).

5 Kholodenko, B. N., Demin, O. V., Moehren, G. & Hoek, J. B. Quantification of short term signaling by the epidermal growth factor receptor. *J. Biol. Chem.* **274**, 30169-30181 (1999).

6 Schoeberl, B., Eichler-Jonsson, C., Gilles, E. D. & Muller, G. Computational modeling of the dynamics of the MAP kinase cascade activated by surface and internalized EGF receptors. *Nat. Biotechnol.* **20**, 370-375 (2002).

7 Levkowitz, G. et al. Ubiquitin ligase activity and tyrosine phosphorylation underlie suppression of growth factor signaling by c-Cbl/Sli-1. *Mol. Cell* **4**, 1029-1040 (1999).

8 Rozakis-Adcock, M. et al. Association of the Shc and Grb2/Sem5 SH2-containing proteins is implicated in activation of the Ras pathway by tyrosine kinases. *Nature* **360**, 689-692 (1992).

9 Wu, Y., Chen, Z. & Ullrich, A. EGFR and FGFR signaling through FRS2 is subject to negative feedback control by ERK1/2. *Biol. Chem.* **384**, 1215-1226 (2003).

10 Jones, N. & Dumont, D. J. Recruitment of Dok-R to the EGF receptor through its PTB domain is required for attenuation of Erk MAP kinase activation. *Curr. Biol.* **9**, 1057-1060 (1999).

11 Starbuck, C. & Lauffenburger, D. A. Mathematical model for the effects of epidermal growth factor receptor trafficking dynamics on fibroblast proliferation responses. *Biotechnol. Prog.* **8**, 132-143 (1992).

12 Kao, S., Jaiswal, R. K., Kolch, W. & Landreth, G. E. Identification of the mechanisms regulating the differential activation of the mapk cascade by epidermal growth factor and nerve growth factor in PC12 cells. *J. Biol. Chem.* **276**, 18169-18177 (2001).

13 Yamada, S., Taketomi, T. & Yoshimura, A. Model analysis of difference between EGF pathway and FGF pathway. *Biochem. Biophys. Res. Commun.* **314**, 1113-1120 (2004).

Table S1b

Molecule-molecule interaction	Reaction number	kf (/s/μM)	kb (/s)	Notes
	1	8.333e-4 *	2.7778e-4	[1]
	2	6.2	6.4e-5	On the basis of[2], further constrained by *in vivo* dynamics of TrkA (Fig. 1c)
	3	1 *		Constrained by *in vivo* dynamics of TrkA (Fig. 1c)
	4	6.3e-4 *		On the basis of[1], further constrained by *in vivo* dynamics of TrkA (Fig. 1c)
	5	4.2e-4 *		On the basis of[1], further constrained by *in vivo* dynamics of TrkA (Fig. 1c)
	6	10	0.2	On the basis of[3], further constrained by *in vivo* dynamics of Ras (Fig. 1f)
	7	5	0.1	On the basis of[3], further constrained by *in vivo* dynamics of Ras (Fig. 1f)
	8	0.1 *		On the basis of[4], further constrained by *in vivo* dynamics of Ras (Fig. 1f)
	9	2 *		On the basis of[5], further constrained by *in vivo* dynamics of Rap1 (Fig. 1f)
	10	0.0022 *		Constrained by *in vivo* dynamics of TrkA (Fig. 1c)
	* denotes /s.			

Enzymatic reaction	Reaction number	Km (μM)	Vmax (/s)	Notes
	1	0.1	0.02	On the basis of[6], further onstrained by *in vivo* dynamics of Ras (Fig. 1f)

Initial concentration	Molecule	CoInit (μM)		Notes
	TrkA	0.061894		[7]
	pro_TrkA	0.020631	constant	[1]

1 Jullien, J., Guili, V., Reichardt, L. F. & Rudkin, B. B. Molecular kinetics of nerve growth factor receptor trafficking and activation. *J. Biol. Chem.* **277**, 38700-38708 (2002).

2 Mahadeo, D., Kaplan, L., Chao, M. V. & Hempstead, B. L. High affinity nerve growth factor binding displays a faster rate of association than p140trk binding. Implications for multi-subunit polypeptide receptors. *J. Biol. Chem.* **269**, 6884-6891 (1994).

3 Farooq, A., Plotnikova, O., Zeng, L. & Zhou, M. M. Phosphotyrosine binding domains of Shc and insulin receptor substrate 1 recognize the NPXpY motif in a thermodynamically distinct manner. *J. Biol. Chem.* **274**, 6114-6121 (1999).

4 Gatti, A. Divergence in the upstream signaling of nerve growth factor (NGF) and epidermal growth factor (EGF). *Neuroreport* **14**, 1031-1035 (2003).

5 Kao, S., Jaiswal, R. K., Kolch, W. & Landreth, G. E. Identification of the mechanisms regulating the differential activation of the mapk cascade by epidermal growth factor and nerve growth factor in PC12 cells. *J. Biol. Chem.* **276**, 18169-18177 (2001).

6 Jones, N. & Dumont, D. J. Recruitment of Dok-R to the EGF receptor through its PTB domain is required for attenuation of Erk MAP kinase activation. *Curr. Biol.* **9**, 1057-1060 (1999).

7 Esposito, D. et al. The cytoplasmic and transmembrane domains of the p75 and Trk A receptors regulate high affinity binding to nerve growth factor. *J. Biol. Chem.* **276**, 32687-32695 (2001).

Table S1c

Molecule-molecule interaction	Reaction number	kf (/s/μM)	kb (/s)	Notes
	1	0.03	0.0168	[1]
	2	10	0.2	[1,2]
	3	0.005 *		[2]
	4	0.002 *		Constrained by *in vivo* dynamics of SOS (Fig. 1d, e)
	5	0.12	0.01	[3]
	6	0.002 *	1.0e-5	Constrained by *in vivo* dynamics of Ras (Fig. 1f)
	7	1.667e-4 *		[4]
	* denotes /s.			

Enzymatic reaction	Reaction number	Km (μM)	Vmax (/s)	Notes
	1	0.02	2	[5]
	2	25.641	1	[6]
	3	1	10	[7]

Initial concentration	Molecule	CoInit (μM)		Notes
	SOS	0.1		[6]
	Grb2	1		[6]
	RasGAP	0.1		[8]
	Ras	0.1		[6]

1 Chook, Y. M., Gish, G. D., Kay, C. M., Pai, E. F. & Pawson, T. The Grb2-mSos1 complex binds phosphopeptides with higher affinity than Grb2. *J. Biol. Chem.* **271**, 30472-30478 (1996).

2 Sasaoka, T., Langlois, W. J., Leitner, J. W., Draznin, B. & Olefsky, J. M. The signaling pathway coupling epidermal growth factor receptors to activation of p21ras. *J. Biol. Chem.* **269**, 32621-32625 (1994).

3 Kuriyan, J. & Cowburn, D. Modular peptide recognition domains in eukaryotic signaling. *Annu. Rev. Biophys. Biomol. Struct.* **26**, 259-288 (1997).

4 Kawata, M. et al. A novel small molecular weight GTP-binding protein with the same putative effector domain as the ras proteins in bovine brain membranes. Purification, determination of primary structure, and characterization. *J. Biol. Chem.* **263**, 18965-18971 (1988).

5 Margarit, S. M. et al. Structural evidence for feedback activation by Ras.GTP of the Ras-specific nucleotide exchange factor SOS. *Cell* **112**, 685-695 (2003).

6 Bhalla, U. S. & Iyengar, R. Emergent properties of networks of biological signaling pathways. *Science* **283**, 381-387 (1999).

7 Gideon, P. et al. Mutational and kinetic analyses of the GTPase-activating protein (GAP)-p21 interaction: the C-terminal domain of GAP is not sufficient for full activity. *Mol. Cell. Biol.* **12**, 2050-2056 (1992).

8 Schoeberl, B., Eichler-Jonsson, C., Gilles, E. D. & Muller, G. Computational modeling of the dynamics of the MAP kinase cascade activated by surface and internalized EGF receptors. *Nat. Biotechnol.* **20**, 370-375 (2002).

Table S1d

Molecule-molecule interaction	Reaction number	kf (/s/μM)	kb (/s)	Notes
	1	1	0.002	[1]
	2	1	0.2	[2]
	3	0.005 *		Constrained by *in vivo* dynamics of Rap1 activation (Fig. 1g)
	4	1.166e-4 *		[3]
	* denotes /s.			

Enzymatic reaction	Reaction number	Km (μM)	Vmax (/s)	Notes
	1	0.01	0.024	On the basis of[4], further constrained by *in vivo* dynamics of Rap1 activation (Fig. 1g)
	2	1	2	[5]

Initial concentration	Molecule	CoInit (μM)		Notes
	C3G	0.5		Constrained by *in vivo* dynamics of Rap1 activation (Fig. 1g)
	Crk	1		Constrained by *in vivo* dynamics of Rap1 activation (Fig. 1g)
	Rap1	0.2		On the basis of[6], further constrained by *in vivo* dynamics of Rap1 activation (Fig. 1g)
	Rap1GAP	0.012		On the basis of[6], further constrained by *in vivo* dynamics of Rap1 activation (Fig. 1g)

1 Knudsen, B. S., Feller, S. M. & Hanafusa, H. Four proline-rich sequences of the guanine-nucleotide exchange factor C3G bind with unique specificity to the first Src homology 3 domain of Crk. *J. Biol. Chem.* **269**, 32781-32787 (1994).

2 Kuriyan, J. & Cowburn, D. Modular peptide recognition domains in eukaryotic signaling. *Annu. Rev. Biophys. Biomol. Struct.* **26**, 259-288 (1997).

3 Kawata, M. et al. A novel small molecular weight GTP-binding protein with the same putative effector domain as the ras proteins in bovine brain membranes. Purification, determination of primary structure, and characterization. *J. Biol. Chem.* **263**, 18965-18971 (1988).

4 Gotoh, T. et al. Identification of Rap1 as a target for the Crk SH3 domain-binding guanine nucleotide-releasing factor C3G. *Mol. Cell. Biol.* **15**, 6746-6753 (1995).

5 Daumke, O., Weyand, M., Chakrabarti, P. P., Vetter, I. R. & Wittinghofer, A. The GTPase-activating protein Rap1GAP uses a catalytic asparagine. *Nature* **429**, 197-201 (2004).

6 Polakis, P. G., Rubinfeld, B., Evans, T. & McCormick, F. Purification of a plasma membrane-associated GTPase-activating protein specific for rap1/Krev-1 from HL60 cells. *Proc. Natl. Acad. Sci. U.S.A.* **88**, 239-243 (1991).

Table S1e

Molecule-molecule interaction	Reaction number	kf (/s/μM)	kb (/s)	Notes
	1	60	0.5	[1]
	2	60	0.5	[1,2]
	3	60	0.5	[3]
	4	0.15 *		[1]
	5	10	0.075	[4]
	6	16.304	0.6	[1]
	* denotes /s.			

Enzymatic reaction	Reaction number	Km (μM)	Vmax (/s)	Notes
	1	0.16	0.5	[1]
	2	0.16	0.2	[1]
	3	0.16	0.3	[1]
	4	15.657	3	[1]
	5	0.02	0.06	[5]

Initial concentration	Molecule	CoInit (μM)		Notes
	c-Raf	0.5		[1]
	B-Raf	0.2		[1]
	MEK	0.68		[1]
	ERK	0.26		[1]
	PP2A	0.24		[1]
	MKP3	0.018		[1,6]

1 Bhalla, U. S. & Iyengar, R. Emergent properties of networks of biological signaling pathways. *Science* **283**, 381-387 (1999).

2 Yamamori, B. et al. Purification of a Ras-dependent mitogen-activated protein kinase kinase kinase from bovine brain cytosol and its identification as a complex of B-Raf and 14-3-3 proteins. *J. Biol. Chem.* **270**, 11723-11726 (1995).

3 Ohtsuka, T., Shimizu, K., Yamamori, B., Kuroda, S. & Takai, Y. Activation of brain B-Raf protein kinase by Rap1B small GTP-binding protein. *J. Biol. Chem.* **271**, 1258-1261 (1996).

4 Khokhlatchev, A. V. et al. Phosphorylation of the MAP kinase ERK2 promotes its homodimerization and nuclear translocation. *Cell* **93**, 605-615 (1998).

5 Zhao, Y. & Zhang, Z. Y. The mechanism of dephosphorylation of extracellular signal-regulated kinase 2 by mitogen-activated protein kinase phosphatase 3. *J. Biol. Chem.* **276**, 32382-32391 (2001).

6 Schoeberl, B., Eichler-Jonsson, C., Gilles, E. D. & Muller, G. Computational modeling of the dynamics of the MAP kinase cascade activated by surface and internalized EGF receptors. *Nat. Biotechnol.* **20**, 370-375 (2002).